

Analysis of nonequilibrium phenomena during interaction of laser radiation with metal vapors

Vladimir I. Mazhukin, Vadim V. Nossov, Moscow, Igor Smurov, Saint-Etienne, and Gilles Flamant, Font-Romeu

Summary. The interaction of laser radiation in the range of intensity between 10^6 and 10^{10} W/cm² and at a wavelength of 1.06 μm with metal vapors is simulated. The collision-radiation model is applied to describe the kinetics of nonequilibrium ionization and recombination. It is shown that the interaction of laser radiation with a vapor can proceed in two qualitatively different ways, namely, the prebreakdown regime and the optical-breakdown regime. If the radiation intensity is insufficient to induce avalanche ionization, the system comes into a stationary state characterized by the thermodynamic equilibrium, the equilibrium between the radiation and the vapor being absent. At higher values of the laser intensity the optical breakdown starts, which is a nonequilibrium transition state from a partially ionized vapor to a fully ionized plasma where Coulomb collisions are predominant. The two metals under consideration, aluminum and copper, are close in their thermo-physical properties but differ in the configuration of the electron shells of their atoms. The optical-breakdown threshold and the onset time are analyzed in relation to the ionization potential, the total number of excited states under consideration, and the positions of lower and higher levels of excitation. It is shown that the radiation intensity threshold in metal vapor depends to a greater extent on the configuration of electronic shells of atom than on the atom ionization potential.

AMS subject classification: 80A30, 7808, 3404.

Keywords: Chemical kinetics; Laser plasma; Stiff system of ordinary differential equations.

1 Introduction

The optical breakdown of an evaporated material near the surface of a solid target is a combination of processes which cause the gaseous medium to qualitatively change its properties. The medium transfers from the state of a partially ionized gas completely transparent for the incident radiation into the state of complete ionization that intensively absorbs laser radiation. Therefore the optical breakdown that constitutes the initial stage of the rapid formation of laser plasma is a subject of particular attention and of thorough studies. There is a considerable amount of experimental and theoretical data on the pulsed action of a moderate intensity G of 10^6 to 10^{10} W/cm² and a relatively long duration τ of 10^{-9} to 10^{-6} s over a wide range of wavelengths λ from 0.238 to 10.6 μm on different materials [1–17]. Both the fundamental and applied aspects of the problem attract considerable interest.

From the fundamental standpoint the phenomenon of optical breakdown is related to general problems of the emergence and development of high-nonequilibrium systems during the interaction of concentrated energy fluxes with matter. One of the central problems which at present has no generally accepted solution is the process of establishing a local thermodynamic equilibrium in a laser-induced plume. Thus, if the state of a plasma in thermodynamic equilibrium is fully determined by its temperature T and density ρ and its charge composition corresponds to the Saha–Boltzmann distribution [18], then in the case of a violation of the local thermodynamic equilibrium the plasma behavior is determined by a combination of kinetic, radiative, and gas-dynamic processes. In such situations major problems are as a rule connected with determining the charge composition and radiative characteristics of the material, which cannot be treated correctly without taking into account the kinetics of ionization-recombination processes. Owing to the strong nonlinearity and interdependence of numerous processes it is hard to predict which of the mechanisms will dominate at different stages of the evolution. Therefore when studying nonequilibrium systems, computational experiments are of great importance along with full-scale experiments. The development and application of appropriate models is an essential part of the present work.

The best-known models describing different states of a low-temperature plasma are the corona model [19, 20], the radiant-thermal-conductivity model [21], and the collision-radiation model [22, 23]. In the framework of the corona model the behavior of an optically transparent plasma of a low density is described quite satisfactorily. The model suggests that the probability of collision-induced jumps between the levels is negligible as compared with the spontaneous decay. As a result, each collision-induced excitation event is compensated by a radiative-decay event. In the corona model the radiation spectrum is represented as a set of narrow lines against the continuous radiation background.

The radiant-thermal-conductivity model is most frequently used to describe a plasma of a great optical thickness and high density. This kind of plasma is characterized by the Saha–Boltzmann distribution of ions and equilibrium black-body radiation containing no lines due to their complete reabsorption.

A plasma of a variable density and an arbitrary optical thickness, in which radiation and collision-induced processes play an essential role, is intermediate between the two above mentioned limiting states and is most difficult to describe [24]. A laser plasma produced near the irradiated surface is an example. To analyze this plasma, different variants of the collision-radiation model are applied. They are supplemented with radiation transfer equations to take into account reabsorption of the linear and continuous spectra.

Placing a solid target in the radiation focal plane makes the situation more complicated because a number of new physical processes come into being. In general, to take them into account one should consider the kinetics of phase transformation in the target, the interaction of evaporation products with the surrounding gaseous atmosphere and new conditions for the occurrence of optical breakdown. The optical-

breakdown initiation in this case is closely connected with the parameters of the evaporated substance, which cannot be known beforehand, depend on the evaporation condition, and can be determined only in the course of solution. Also, the appearance of plasma formations results in a radical change of optical and thermodynamic characteristics of the gaseous medium. In earlier studies [25], the plasma initiation has been identified with phenomena of full or partial screening of the target due to a sharp increase in the optical thickness of the evaporated substance. In later studies [26, 27] the influence of the gas-dynamic factor has been clarified and estimated. Mathematical modeling has shown [28, 29] that high pressure of the plasma can effectively inhibit the evaporation process even to the point of full termination, although the surface temperature T_S remains much higher than the boiling temperature under the normal conditions T_B . Nevertheless, the problem of the plasma–target surface interaction under evaporation conditions has not been completed. As a rule, the equilibrium approximations have been used [30–33], with the range of applicability being much narrower than the entire complex of the phenomena under consideration. The most complicated part of the problem appears to be the determination of interrelations between processes of the micro- and macro-levels. Therefore, despite many attempts to describe mathematically the processes under discussion, there is now no generally recognized physical-mathematical model, that would self-consistently describe the behavior of condensed and gaseous media and take micro-level processes into account: kinetics of nonequilibrium phase transitions and nonequilibrium avalanchelike ionization and recombination of gas and vapor atoms. A full and correct consideration of initiation and expansion of nonequilibrium laser plasma in the evaporated substance can be performed only in the nonequilibrium radiative-gas dynamic approximation. This approximation includes the collision-radiation model of nonequilibrium kinetics as one of the most important components. To develop models of this type is an important scientific problem for theoretical investigations of plasma.

Applied aspects of the optical-breakdown problem are connected mainly with different technological regimes of material treatment with concentrated energy fluxes. In the so-called technological range of intensity $G \leq 10^9 \text{ W/cm}^2$, the laser plasma can exert both a positive and a negative influence. Useful plasma effects are revealed when the plasma is employed as a chemically active medium to synthesize carbides and nitrides of various metals [34]. Laser plasma can be applied to increase the energy input into the target due to the phenomenon of plasma reradiation in another spectral range that can lead to a significant increase of the total target absorption [35]. The laser-induced plume containing ionized and neutral particles is used in pulsed laser deposition [36, 37]. Laser-induced plasma spectra can be used to analyze the chemical composition of a medium [38, 39].

A negative plasma influence is revealed mainly in the plasma screening action of plasma that hinders a direct delivery of the laser radiation energy onto the surface to be treated.

Thus, optical-breakdown studies are important from the standpoint of monitor-

ing and control of laser action on materials. Although there is a great amount of theoretical and experimental works, so far there are no well-established concepts accounting for all the aspects of the problem. Breakdown mechanisms, their changes and interactions are not ultimately clear. At the same time, however, analysis of the available data shows that the measured values of the threshold intensity and the breakdown duration turn out to be much lower than the theoretical ones.

The main objective of the present study is to develop and to comprehensively study the collision-radiation model that describes the kinetics of nonequilibrium ionization and recombination for the laser plasma of an arbitrary density and optical thickness. This model is used to study and compare the avalanche ionization process in vapors of two metals, aluminum and copper, which have similar thermophysical characteristics (in particular, the evaporation parameters) and comparable ionization potentials of neutral atoms but different structures of electron shells of atoms and ions.

The performed modeling of the optical-breakdown kinetics shows that the laser action duration and the evaporated-substance temperature are the main parameters that influence the threshold intensities of optical breakdown. It is also found that the electronic shell structure of the atom plays a more important role than the ionization potential. This fact has not been mentioned before. Comparative analysis of the optical breakdown in Al and Cu vapors shows that atoms with lowly positioned excited states (Cu) have higher threshold values of the radiation intensity. The important role of the electronic configuration imposes rigorous demands on the description of the population kinetics that depends on the number of excited levels taken into account. Correct kinetic models for metal atoms should include at least 10 excited states.

2 Statement of the problem

Consider the laser action on the surface of a metal target with a flat-top temporal pulse shape and an intensity sufficient to maintain the intensive evaporation. According to the conventional concepts, the intensive surface evaporation into vacuum can be described using the approximation of the nonequilibrium Knudsen layer adjacent to the evaporated surface [40]. Macroscopically, the Knudsen layer is a gas-dynamic gap at which the main parameters, i.e., the temperature T , the density ρ and the pressure P of the medium, undergo a discontinuous change. It is supposed that passing through the Knudsen layer, the local thermodynamic equilibrium has time to be set in the ablation flow, and Saha–Boltzmann equations can be used to determine the initial concentrations of electrons and ions in the ground and excited states. In the present study the stages of heating and evaporating the target are not considered.

The initial values of the temperature T_0 and the vapor density ρ_0 are selected on the following grounds: they are to be found in the region of the condensed-medium–vapor phase transition; to correspond to the data for the outer side of the Knudsen layer; to provide an electron concentration low enough to absorb a considerable amount of the incident laser radiation. In particular, these requirements are met if

the (T_0, ρ_0) pair selected corresponds to the boiling temperature T_B under normal conditions. Later on, with a sufficient radiation intensity, the conditions for the avalanche ionization (optical breakdown) in the material vapor can be realized as a result of electron gas heating due to the inverse-bremsstrahlung effect.

2.1 *The unsteady-state collision-radiation model*

A great number of various elementary events and processes take place in the interaction of the evaporated material with laser radiation, and the character of the macroprocess is determined by their combination. The kinetics of collision-radiation transitions and the ionization of aluminum and copper vapors are described with the help of the unsteady-state collision-radiation model. This model accounts for those reactions only which make the greatest contribution within the considered energy range. As for radiation transitions, those reactions which are represented by the most intensive lines in the corresponding spectrum are taken into account.

Note two important facts to be accounted for by the collision-radiation model describing the laser plasma dynamics. The first one is the violation, at some stages, of the local thermodynamic equilibrium. This may occur both during the action of the laser pulse and on completion of the pulse. During the laser pulse action the translational temperature T_e becomes higher than the translational temperature T_g of atoms and ions due to absorption of electromagnetic radiation by electrons and a significant difference between the mass of the electron m and that of heavy particles (ions and neutral atoms) M . The plasma produced turns out to be overheated, i.e., in the state of ionizational nonequilibrium. At this state the average charge of the plasma is smaller than the equilibrium one, and the concentrations of charged particles and excited states differ (by being smaller) from the Saha–Boltzmann distribution [41].

On completion of the laser action, the stage of inertial gas-dynamic expansion begins and for a sufficiently high expansion rate the plasma may become undercooled or recombinationally nonequilibrium [42]. In such a state the relations characterizing the degree of deviation from the equilibrium will be inverse as compared to the overheated state.

Therefore the laser plasma collision-radiation model must include, in addition to the kinetics equations, two energy balance equations: for the electron and for heavy-particle systems.

The second fact to be taken into account when developing the mathematical model is that the energy levels of atoms and ions in metals are, as a rule, split and mixed, therefore a great number of excited levels and collision-radiation transitions should be included into the model.

The main assumptions of the present model are:

- a monatomic plasma of one chemical element is considered;
- at the initial state the metal vapor consists of atoms, ions and electrons which are in complete thermodynamic equilibrium;

- spatial effects are not considered: all kinds of radiation except for laser freely leave the system;
- the experimentally determined average electron energy does not exceed 10 to 20 eV for the regimes considered, ions with higher ionization potentials are not taken into consideration;
- photo-processes are not taken into account.

The mathematical models describing the level-by-level kinetics and ionization of aluminum and copper have differences owing to the electron configuration of atoms [43].

At the unfilled shell of an aluminum atom there are three electrons $1s^2 2s^2 2p^6 3s^2 3p$ with relatively low ionization potential, namely, $J_0^0 = 5.986$ eV, $J_0^1 = 18.8$ eV, and $J_0^2 = 28.448$ eV. Electrons of the filled shell $1s^2 2s^2 2p^6$ have a high ionization potential, for example, $J_0^3 \simeq 120$ eV. Therefore due to above mentioned energy restriction, the collision-radiation model of aluminum includes the kinetics of the neutral atom Al ($z = 0$) and the first two ions Al^+ ($z = 1$) and Al^{++} ($z = 2$), where z is the ionization factor. The neon-like ion Al^{+++} ($z = 3$) is taken to have no structure and is included in the form of a nucleus.

The electron structure of the copper atom differs much from that of the aluminum atom. In the unfilled shell of Cu $1s^2 2s^2 2p^6 3s^2 3p^6 3d^{10} 4s$ (2S) there is one electron with the ionization potential $J_0^0 = 7.72$ eV. Then there is the d -shell, whose outer electrons have comparatively low potentials $J_0^1 = 20.291$ eV and $J_0^2 = 36.834$ eV. However, electron transitions of the d -shell are characterized by a low radiating power and their radiative characteristics are poorly known. For this reason the collision-radiation model of the copper atom includes the kinetics of the neutral Cu atom and the first ion Cu^+ ($z = 1$). The second ion Cu^{++} ($z = 2$) with $J_0^2 = 20.291$ eV is included in the model in the form of a nucleus.

2.2 Elementary phenomena and transitions in the atom

Major elementary phenomena taken into account in the collision-radiation model are listed below.

Spontaneous radiative decay of excited states of atoms and ions:

$$n_m^z \xrightarrow{A_{mj}^z} n_j^z + \hbar\omega, \quad (1)$$

where A_{mj}^z [s^{-1}] is the constant of radiation transition rate that differs from zero only for optical transitions permitted by the selection rules for the z -charged particle. Hereinafter in variables with a double subscript the first index denotes the initial state of transition and the second one denotes the final state.

Excitation and deexcitation of atoms and ions by an electron impact:

$$n_m^z + e \xrightleftharpoons[r_{jm}^z]{k_{mj}^z} n_j^z + e, \quad (2)$$

where k_{mj}^z [$\text{cm}^3 \cdot \text{s}^{-1}$] is the excitation reaction rate for the (m, j) collisional transition of a particle with the charge z and r_{jm}^z is the deexcitation reaction rate for the inverse transition. The index j assumes the values corresponding to the level numbers where the z -charged particles from the m -level can pass into, in accordance with the quantum-mechanical selection rules.

Ionization of the ground and excited states of atoms and ions by the electron impact:

$$n_m^z + e \xrightarrow{\alpha_m^z} n_0^{z+1} + e + e, \quad (3)$$

where α_m^z [$\text{cm}^3 \cdot \text{s}^{-1}$] is the ionization rate constant of the m th level of the z -charged particle, the ionization being induced by the electron impact.

Three-particle recombination, i.e., a reaction inverse to the impact ionization (the third particle is the electron):

$$n_0^{z+1} + e + e \xrightarrow{\beta_m^z} n_m^z + e, \quad (4)$$

where β_m^z [$\text{cm}^6 \cdot \text{s}^{-1}$] is the reaction rate constant.

Tables 1 and 2 represent the ground and excited states of neutral atoms and ions of Al and Cu that are taken into account in the model. Figures 1–5 show the collision and radiation transitions under consideration.

Table 1. Excited levels of neutral atom and ions of Al included in the model

Al		Al ⁺		Al ⁺⁺	
$1s^2 2s^2 2p^6 3s^2 3p$	$(^2P^0)$	$1s^2 2s^2 2p^6 3s^2$	(^1S)	$1s^2 2s^2 2p^6 3s$	(^2S)
$4s$	(^2S)	$3s 3p$	$(^1,3P^0)$	$3p$	$(^2P^0)$
$3d$	(^2D)	$3s 4s$	$(^1,3S)$	$3d$	$(^2P^0)$
$4p$	$(^2P^0)$	$3s 3d$	$(^1,3D)$	$4s$	(^2S)
$5s$	(^2S)	$3s 4p$	$(^1,3P^0)$	$4p$	$(^2P^0)$
$4d$	(^2D)	$3s 4d$	$(^1,3D)$	$4d$	(^2D)
$5p$	$(^2P^0)$	$3s 6$		$4f$	(^2D)
$4f$	$(^2F^0)$	$3s 7$		$5s$	(^2S)
$6s, p$	$(^2S, ^2P^0)$	$3s 8$		$5p$	$(^2P^0)$
$5d$	$(^2D^0)$			$5d$	$(^2P^0)$
$6f$	$(^2F^0)$			$5f$	$(^2F^0)$
$6d, f$	$(^2D, ^2F^0)$			$2p^{67}$	
$3s^2(7-10)$				$2p^{68}$	
				$2p^{69}$	

Table 2. Excited levels of neutral atom and ion of Cu included in the model

Cu		Cu ⁺	
$3s^2 3p^6 3d^{10} 4s$	(² S)	$3s^2 3p^6 3d^{10}$	(² S)
$4s^2$	(² D)	$4s$	(^{1,3} D)
$4p'$	(^{2,4} P ⁰ , ² F ⁰ , ^{2,4} D ⁰)	$4p$	(¹ P ⁰ , ^{1,3} D ⁰ , ³ F ⁰)
$4d$	(² D)	$5s$	(³ D)
$5s$	(² S, ⁴ D)	$5p$	(³ D, ³ G, ³ F, ³ F ⁰ , ³ P ⁰)
$5p$	(² P ⁰)	$6s$	(³ D)
$5d$	(² D)	$3d^{10} 8$	
$6p$	(² P ^o)	$3d^{10} 9$	
$7p$	(² P ^o)	$3d^{10} 10$	
$3d^{10} 8$			
$3d^{10} 9$			
$3d^{10} 10$			

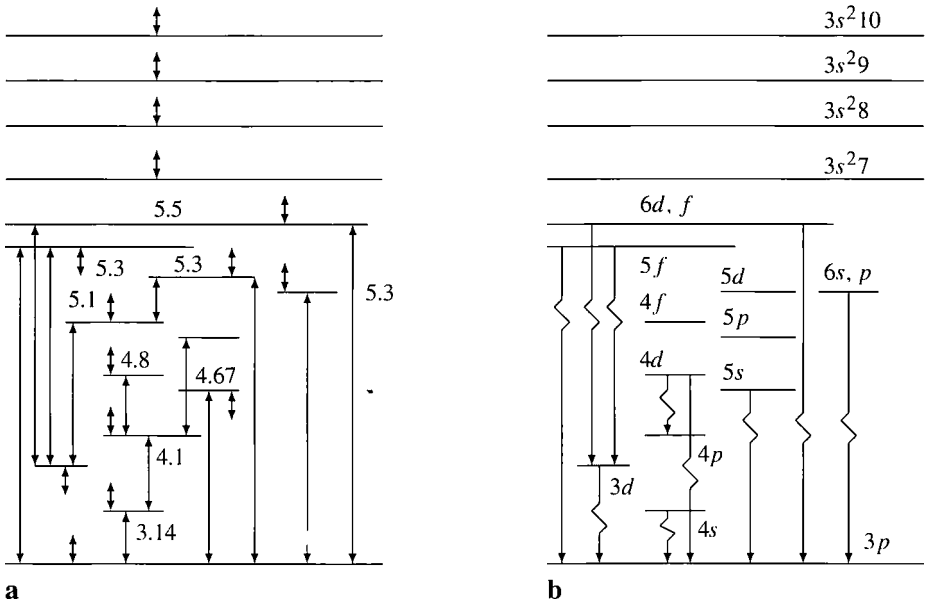


Fig. 1. Diagrams of permitted collision (a) and radiation (b) transitions for neutral atom of Al, ionization potential $J_0^0 = 5.986$ eV. **a** The arrows $\uparrow\downarrow$ indicate that level can be either ionized by electron impact or formed by three-particle recombination; the numbers denote ionization potential of excited levels

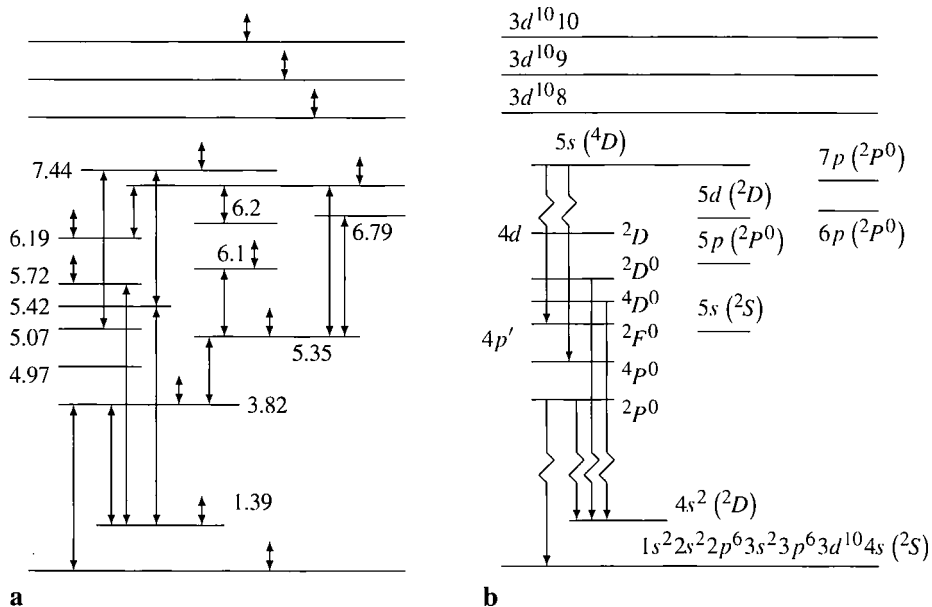


Fig. 4. Diagrams of permitted collision (a) and radiation (b) transitions for neutral atom of Cu, ionization potential $J_0^0 = 7.726$ eV. **a** The arrows \updownarrow indicate that level can be either ionized by electron impact or formed by three-particle recombination; the numbers denote ionization potential of excited levels

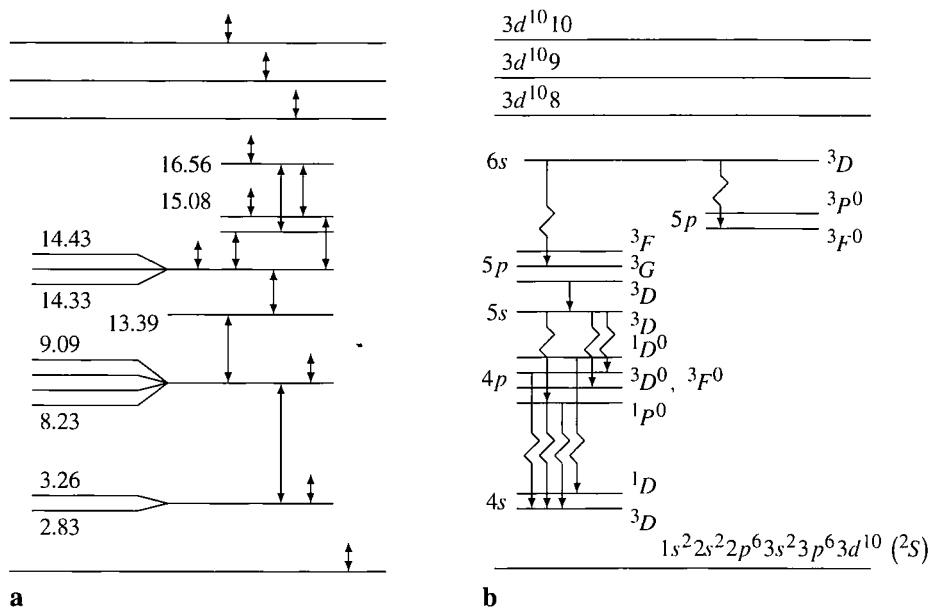


Fig. 5. Diagrams of permitted collision (a) and radiation (b) transitions for Cu^+ , ionization potential $J_0^1 = 20.291$ eV

2.3 The system of equations

The ion distribution evolution and the level-by-level kinetics of neutral atoms and ions are described by the following system of nonlinear differential equations.

For the ground state of the neutral atom ($z = 0$):

$$\frac{\partial N_0^0}{\partial t} = - \sum_{j=1}^{M^0} (k_{0j}^0 N_0^0 - r_{j0}^0 N_j^0) N_e + \sum_{j=1}^{M^0} A_{j0}^0 N_j^0 - (\alpha_0^0 N_0^0 - \beta_0^0 N_0^1 N_e) N_e. \quad (5)$$

For the ground state of z -charged ions ($z = 1, 2, \dots, z_{\max} - 1$):

$$\begin{aligned} \frac{\partial N_0^z}{\partial t} = & - \sum_{j=1}^{M^z} (k_{0j}^z N_0^z - r_{j0}^z N_j^z) N_e + \sum_{j=1}^{M^z} A_{j0}^z N_j^z \\ & + \sum_{j=0}^{M^{z-1}} (\alpha_j^{z-1} N_j^{z-1} - \beta_j^{z-1} N_0^z N_e) N_e - (\alpha_0^z N_0^z - \beta_0^z N_0^{z+1} N_e) N_e. \end{aligned} \quad (6)$$

For excited states of the neutral atom and ions ($m = 1, \dots, M^z$; $z = 0, \dots, z_{\max} - 1$):

$$\begin{aligned} \frac{\partial N_m^z}{\partial t} = & + \sum_{j=0}^{m-1} (k_{jm}^z N_j^z - r_{mj}^z N_m^z) N_e - \sum_{j=m+1}^{M^z} (k_{mj}^z N_m^z - r_{jm}^z N_j^z) N_e \\ & + \sum_{j=m+1}^{M^z} A_{jm}^z N_j^z - \sum_{j=0}^{m-1} A_{mj}^z N_m^z - (\alpha_m^z N_m^z - \beta_m^z N_0^{z+1} N_e) N_e. \end{aligned} \quad (7)$$

For the ion with $z = z_{\max}$:

$$\frac{\partial N_0^{z_{\max}}}{\partial t} = \sum_{j=0}^{M^{z_{\max}-1}} (\alpha_j^{z_{\max}-1} N_j^{z_{\max}-1} - \beta_j^{z_{\max}-1} N_0^{z_{\max}} N_e) N_e. \quad (8)$$

For the electrons:

$$\frac{\partial N_e}{\partial t} = \sum_{z=1}^{z_{\max}} \sum_{m=0}^{M^z} \frac{\partial N_m^z}{\partial t}. \quad (9)$$

In the system (5)–(9), N_m^z is the density of the z -charged particles in the m -state, N_e is the density of free electrons. M^z denotes the number of excited states of the z -charged particle included in the model, $M^{z_{\max}} = 0$; z_{\max} is the maximum degree of ionization of the neutral atom. For the Al vapor $z_{\max} = 3$, and for the Cu vapor $z_{\max} = 2$, the particle having the maximum ionization degree is taken to have no structure, i.e., its excited states are neglected.

From the energy exchange viewpoint, in the low-temperature monatomic plasma it is possible to distinguish three subsystems associated with: the inner degrees of freedom of atoms and ions, the translational degrees of free electrons, and the trans-

lational degrees of heavy particles. Within each subsystem the energy exchange proceeds most rapidly. Energy exchange between the translational degrees of freedom proceeds most slowly. As mentioned above, this is connected with a great difference between the mass of the electron and that of the heavy particle (an atom or an ion). Consequently, it is only a small portion of the kinetic energy of colliding particles that can be transmitted by one collision [44]: $\delta \simeq 2m/M$. Therefore the energy balance of the nonequilibrium plasma is characterized by two temperatures: T_e for the electronic component and T_g for the heavy particles.

The equations for the energy balance of the translational degrees of freedom of the electrons and heavy particles are written in the following form [44]:

$$\frac{d}{dt} \left(\frac{3}{2} N_e T_e \right) = \left\{ G\mu - \frac{3}{2} \delta (T_e - T_g) \right\} (\nu_{en} + \nu_{ei}) N_e - \sum_{z=0}^{z_{\max}-1} \sum_m^{M^z} Q_{z,m}^J - \sum_{z=0}^{z_{\max}-1} \sum_m^{M^z-1} Q_{z,m}^{\Delta E}, \quad (10)$$

$$N_g \frac{dT_g}{dt} = \delta (T_e - T_g) (\nu_{en} + \nu_{ei}) N_e, \quad N_g = \sum_{z=0}^{z_{\max}} \sum_{m=0}^{M^z} N_m^z. \quad (11)$$

The parameter μ characterizes the energy portion gained by the electron in the laser radiation electromagnetic field during one collision with an atom or an ion,

$$\mu = \frac{4\pi e^2}{mc(\omega^2 + (\nu_{en} + \nu_{ei})^2)}.$$

Here $\omega = 4\pi\nu$ is the incident radiation frequency, ν_{en} is the frequency of electron-neutral collisions, ν_{ei} is the frequency of electron-ion collisions, c denotes the speed of light, and e is the charge of the electron.

During inelastic collisions including elementary reactions of excitation, deexcitation, ionization and recombination, the energy exchange is characterized by the terms:

$$Q_{z,m}^{\Delta E} = \sum_{j=m+1}^{M^z} \Delta E_{mj}^z (k_{mj}^z N_m^j - r_{jm}^z N_j^z) N_e, \quad (12)$$

$$Q_{z,m}^J = J_m^z (\alpha_m^z N_m^z - \beta_m^z N_0^{z+1} N_e) N_e, \quad (13)$$

where $Q_{z,m}^{\Delta E}$ takes account of the energy exchange due to excitation and deexcitations reactions of the m th level in the atom or ion; $Q_{z,m}^J$ takes account of the energy exchange due to ionization and three-particle recombination. The ionization energy of the m th state ($m \neq 0$) is calculated as $J_m^z = J_0^z - \Delta E_{0m}^z$, where ΔE_{0m}^z denotes the excitation energy of the m th level of the z -charged particle, and J_0^z is the ionization energy of the ground state.

Note that in contrast to the energy equation for electrons, the energy balance

equation for heavy particles does not include the term dN_g/dt that represents the rate of change in the concentration of heavy particles, since this concentration remains constant under the assumption of the monatomic plasma of one chemical element.

Thus, the energy balance equations (10) and (11), together with the equations for populations and charge composition of the excited levels (5)–(9), form a closed system describing the dynamics of processes in the nonequilibrium spatially homogeneous laser plasma.

2.4 Saha–Boltzmann equations

To estimate quantitatively the degree of nonequilibrium, the concentrations of neutral atoms, charged and excited particles found as a solution of the system (5–11) are compared with the equilibrium concentrations calculated for the temperatures T_e and T_g . The equilibrium values of the concentrations of ions $N_0^{z,\text{Saha}}$ and electrons N_e^{Saha} are determined from the solution of the Saha–Boltzmann system of equations [23]:

$$\frac{N_e^{\text{Saha}}(T_k) \sum_{m=0}^{M^{z+1}} [N_m^{z+1,\text{Saha}}(T_k)]}{\sum_{m=0}^{M^z} [N_m^{z,\text{Saha}}(T_k)]} = \frac{g_e g^{z+1}}{g^z} \left\{ \frac{m T_k}{2\pi \hbar^2} \right\}^{3/2} \exp\left(-\frac{J_0^z}{T_k}\right), \quad (14)$$

$$z = 0, 1, \dots, z_{\text{max}} - 1, \quad T_k \in \{T_e, T_g\} \quad (15)$$

where g_e is the statistical weight of the electron, g^z is the statistical sum of the z -charged particle, and g_m^z is the statistical weight of the m th state of the z -charged particle.

Populations of excited levels are estimated via the ground state concentrations N_0^z , using the Boltzmann relations:

$$N_m^z = N_0^z \exp\left(-\frac{\Delta E_{0m}^z}{k T_k}\right) \frac{g_m^z}{g_0^z}. \quad (16)$$

3 Reaction rates and numerical solution

3.1 Determination of the rate coefficients

When constructing the mathematical model, special attention is paid to the correct determination of the rate coefficients of elementary events. There are several methods of solving this problem. Within the range of high energies of colliding particles of $\varepsilon \geq 100$ eV the calculations of the cross section by classical and quantum-mechanical approaches are in a good agreement with experimental data [45–48]. The determination of elementary reaction rates in the low-energy range of $\varepsilon < 10$ eV is the most difficult. In this case, results of experimental measurements of cross sections and reaction rates are usually used. But such data are available for a limited number of elementary processes only. Moreover, the values of cross sections reported

in experimental papers largely differ from each other. In the present paper, the approximate expressions developed in view of theoretical and experimental studies [49–54] are used to calculate the rate coefficients.

As for the rates of spontaneous radiative decay, either the reference data are used [54, 55] or if the latter are not available, the decay probabilities are determined via the oscillator strengths f_{mj}^z

$$A_{mj}^z = 8 \cdot 10^5 \left\{ \frac{\Delta E_{mj}^z}{\text{Ry}} \right\}^2 \frac{g_m^z}{g_j^z} f_{mj}^z \quad [\text{s}^{-1}], \quad (17)$$

where f_{mj}^z is the oscillator strength for the transition from the m th state to the j -state in the z -charged particle, g_m^z and g_j^z are the statistical weights of the m and j atomic levels for the z -charged particle, Ry is the Rydberg constant.

If the reference data on the oscillator strengths are neither available, their values are estimated by the hydrogen-like dipole moment $f_{mj}^{z,(H)}$ [56]

$$f_{mj}^z = f_{mj}^{z,(H)} \frac{g_m^{z,(H)}}{g_j^z} \frac{\Delta E_{mj}^z}{\Delta E_{mj}^{z,(H)}},$$

where the index H denotes the corresponding values in the hydrogen atom or ion.

The value ν_{en} is determined via the cross section σ of elastic collisions of electrons with neutral atoms and the mean velocity of thermal motion of electrons \bar{v}_e ,

$$\bar{v}_e = 6.7 \cdot 10^7 \sqrt{T_e} \quad [\text{cm} \cdot \text{s}^{-1}], \quad \sigma = 10^{-15} / \sqrt{T_e} \quad [\text{cm}^2].$$

Thus, we have:

$$\nu_{\text{en}} = \bar{v}_e \sigma \sum_{m=0}^{M^0} N_m^0 = 6.7 \cdot 10^{-8} \sum_{m=0}^{M^0} N_m^0 \quad [\text{s}^{-1}]. \quad (18)$$

The frequency of electron–ion collisions is determined by the formula:

$$\nu_{\text{ei}} = 3.64 \cdot 10^{-6} \ln \lambda T_e^{-3/2} \sum_{z=1}^{z_{\text{max}}} \sum_{m=0}^{M^z} N_m^z \quad [\text{s}^{-1}], \quad (19)$$

where $\ln \lambda$ is the Coulomb logarithm.

The constants of excitation reaction rates for atoms and ions are determined with the help of the Van Regemorter approximation formula [53]:

$$k_{mj}^z = 1.58 \cdot 10^{-5} \frac{f_{mj}^z}{\Delta E_{mj}^z \sqrt{T_e}} \exp \left\{ \frac{\Delta E_{mj}^z}{T_e} \right\} Q_{mj}^z \quad [\text{cm}^3 \cdot \text{s}^{-1}], \quad (20)$$

Q_{mj}^z is the Mewe factor:

$$Q_{mj}^z = A + Cx_{mj}^z + \left[Bx_{mj}^z - C(x_{mj}^z)^2 + D \right] \exp\left\{ \frac{\Delta E_{mj}^z}{T_e} \right\} Ei(x_{mj}^z),$$

$$x_{mj}^z = \Delta E_{mj}^z / T_e,$$

where Ei is the integral exponent; the values A , B , C , and D are the constants and are determined by the type of electron transition (dipole, quadrupole, etc.), their values being given in ref. [57].

The inverse values, the deexcitation reactions rates, are calculated from the detailed balance relations:

$$r_{jm}^z = k_{mj}^z \frac{g_j^z}{g_m^z} \exp(-x_{mj}^z). \quad (21)$$

The ionization reaction rates for atoms and ions are calculated with the help of the Lotz formula [51, 52]:

$$\alpha_m^z = 3.14 \cdot 10^{-6} \frac{\xi_m^z Ei(x_m^z)}{T_e^{3/2} x_m^z} \exp(-x_m^z) \text{ [cm}^3 \cdot \text{s}^{-1}\text{]}, \quad (22)$$

where $x_m^z = J_m^z / T_e$ and ξ_m^z is the number of equivalence electrons in the m th state of the z -charged particle.

In the given statement of the problem, three-particle recombination is reciprocal to collision ionization. The rate coefficient for this reaction is calculated from the detailed balance relation [44]:

$$\beta_m^z = \alpha_m^z \cdot \frac{g_m^z}{g_e g_0^{z+1}} \left\{ \frac{2\pi \hbar^2}{m T_e} \right\}^{3/2} \exp(x_m^z) \text{ [cm}^6 \cdot \text{s}^{-1}\text{]}. \quad (23)$$

3.2 Quasicontinuum

Formally speaking, any atom or ion has an infinite number of discrete excited states since the value of the main quantum number is not limited in the Coulomb field. On the other hand, in real models the number of excited states must be finite. An awkward question arises: what number of excited states should be taken into account. There is no general rule to limit this number, therefore, when solving given problems one should bear in mind what properties of the medium are examined and what contribution to these properties is made by highly excited states, along with that made by free electrons. Taking into account that beginning from a certain excited state number M^z , the properties of bound electrons are similar, in the context of macroscopic analysis, to those of free electrons, it is reasonable to associate them with a continuous spectrum. So the states with the numbers $m > M^z$ will be considered in conjunction with a continuous spectrum. By analogy with refs. [41] and [58] they will be named the quasicontinuum. Note that the introduction of the

quasicontinuum is equivalent to the effective reduction of the ionization potential by the value $J_{M^z+1} = \text{Ry}/(M^z + 1)^2$.

Needless to say that for different problems the values of M^z may be essentially different and in general they depend on a number of parameters. The simplest way of solving this problem is to find M^z with the help of preliminary calculations. First, the energy limit for the quasicontinuum should be determined. The quasicontinuum lower limit is found from the assumption that the energy of transition between two neighboring levels $\Delta E_{M^z, M^z+1}^z = J_{M^z+1}^z - J_{M^z}^z$ is much lower than the electron component temperature T_e . This assumption, together with the hydrogen similarity of the levels constituting the quasicontinuum, provides the following criterion for the lower limit:

$$\Delta E_{M^z, M^z+1}^z = \frac{2\text{Ry}}{(M^z + 1)^3} < T_e \implies J_{M^z+1}^z = \text{Ry} \left(\frac{T_e}{2\text{Ry}} \right)^{2/3}, \quad \text{Ry} = 13.6 \text{ eV}.$$

As the density (or the optical thickness) of plasma increases, the quasi-continuous spectrum yields the correct limiting transition to the Saha–Boltzmann distribution. Account of the quasicontinuum effect on lower-excited states is taken by calculating the additional terms $\tilde{\alpha}_m^z$ and $\tilde{\beta}_m^z$ for $m = 0, \dots, M^z$ and $z = 0, \dots, z_{\max} - 1$, for the rates of ionization and three-particle recombination:

$$\hat{\alpha}_m^z = \alpha_m^z + \tilde{\alpha}_m^z, \quad \hat{\beta}_m^z = \beta_m^z + \tilde{\beta}_m^z.$$

The value $\tilde{\alpha}_m^z$ means the reaction rate for electron transition from the m th state in the z -charged particle to the quasicontinuum, and $\tilde{\beta}_m^z$ is the inverse value, i.e., the rate of the electron coming back from the quasicontinuum to the m th state. These values are connected by the relation of the detailed balance. Taking into account that the quasicontinuum consists of high energy levels, the discrete properties of these levels are weakly shown, the recombination flow across discrete states can be determined by means of the diffusion approximation [59]. According to this approximation, the rate of recombination from the quasicontinuum to the m th level $\tilde{\beta}_m^z$ can be expressed as:

$$\tilde{\beta}_m^z = 10^{-27} \frac{(x_m^z)^2 m}{g_c g^z T_e^3} e^{x_m^z} \{ \Phi(x_m^z) - \Phi(x_m^z - x_{M^z+1}^z) \} [\text{cm}^6 \cdot \text{s}^{-1}], \quad (24)$$

$$\Phi(x) = \frac{e^{-x}}{9} \left[\frac{-2 + x - x^2}{x^3} + e^x \text{Ei}(x) \left(1 - \frac{3}{x^3} \right) \right], \quad \text{Ei}(x) = - \int_{-x}^{\infty} e^{-t} \frac{dt}{t},$$

$$\tilde{\alpha}_m^z = \tilde{\beta}_m^z \cdot 6.06 \cdot 10^{21} T_e^{3/2} e^{-x_m^z} \frac{g^z}{g_m^z} [\text{cm}^3 \cdot \text{s}^{-1}], \quad x_m = J_m / T_e, \quad (25)$$

$$m = 0, \dots, M^z, \quad z = 0, \dots, z_{\max}.$$

Hereinafter the values $\hat{\alpha}_m^z$ and $\hat{\beta}_m^z$ are used to denote the modified rates of ionization and recombination. The circumflex accent is omitted.

3.3 Numerical approach

The system of nonlinear differential equations (5)–(11) describes phenomena of different scale whose characteristic times differ by several orders of magnitude. In the general case, such systems of equations are referred to as stiff systems, i.e., systems whose solution contains quickly as well as slowly varying components. The difficulties involved in solving stiff systems are well known [60, 61]. At present there is a thoroughly developed theoretical basis for solving such systems of large dimensions [62], including those with variable stiffness [63]. They are practically realized in various software packages widely used in solving a number of applied problems [64–67].

The above discussed system (5)–(13) is solved numerically with the help of the LASTEC-4 package of applied programs [31] developed by the authors to solve the problems of nonequilibrium radiative-gas dynamics. The software is based on a modification of the Gear–Adams method that belongs to the class of multistep predictor-corrector methods. Similar to ref. [61], the software allows for automatic selection of an integration step and switching from the Gear stiff method to the Adams nonstiff one.

The system of nonlinear algebraic equations of Saha is solved with the help of a special iteration procedure with a high convergence rate [68].

4 Results and analysis

The principal aim of modeling is to study dynamics and general features of nonequilibrium processes taking place in metal vapors under the action of laser radiation of various intensity.

The optical-breakdown dynamics is conveniently characterized by the relation of the frequencies of electron–neutral ν_{en} and Coulomb ν_{ei} collisions. According to ref. [63], a medium with $\nu_{en} \gg \nu_{ei}$ refers to a partially ionized gas, and a medium having the inverse relation $\nu_{en} \ll \nu_{ei}$ is a plasma, i.e., a totally ionized gas. Thus the phenomenon of optical breakdown can be treated as a transition between these two states and is characterized by a sharp increase of ν_{ei} from the initial value that is much smaller than ν_{en} up to the final value that is much greater than ν_{en} .

The optical breakdown of gaseous media is well known to have a pronounced threshold nature as for the intensity and duration of the laser action.

Consider the behavior of vapors of aluminum and copper under the action of laser radiation at the wavelength $\lambda = 1.06 \mu\text{m}$ and near threshold values of intensity. The laser action duration τ varies from 10^{-8} s to 1 s and the intensity G varies within the range of 10^6 to 10^9 W/cm² for the aluminum vapor and 10^7 to 10^{10} W/cm² for the copper vapor. The above mentioned values of G and τ coincide with the data of experimental observation of the plasma formation.

The evaporation of aluminum and copper under normal conditions is characterized

by close values of the boiling temperature T_b and the latent heat of evaporation L_b :

$$T_b^{\text{Al}} = 2793 \text{ K}, L_b^{\text{Al}} = 292 \text{ kJ/mol}; T_b^{\text{Cu}} = 2816 \text{ K}, L_b^{\text{Cu}} = 300 \text{ kJ/mol}.$$

The initial values of the vapor temperature and density for both metals are taken to be typical for the outer side of the Knudsen layer under the conditions of intensive surface evaporation [40]:

$$T_{c,0} = T_{g,0} = T_0 = 0.2 \text{ eV}, \\ N_0^0(\text{Al}) = 6.0 \cdot 10^{18} \text{ cm}^{-3}, N_0^0(\text{Cu}) = 8.3 \cdot 10^{17} \text{ cm}^{-3}.$$

The corresponding equilibrium densities of electrons and ions are:

$$N_e^{\text{Saha}}(\text{Al}) = 4 \cdot 10^{13} \text{ cm}^{-3}, N_e^{\text{Saha}}(\text{Cu}) = 5 \cdot 10^{11} \text{ cm}^{-3}.$$

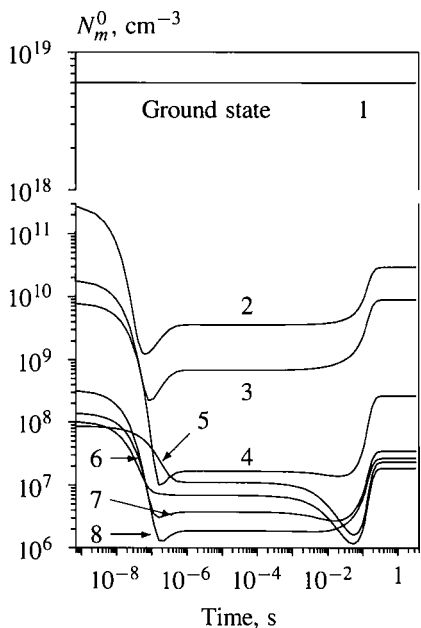
The equilibrium densities of excited states are determined from relation (16).

4.1 The prebreakdown regime

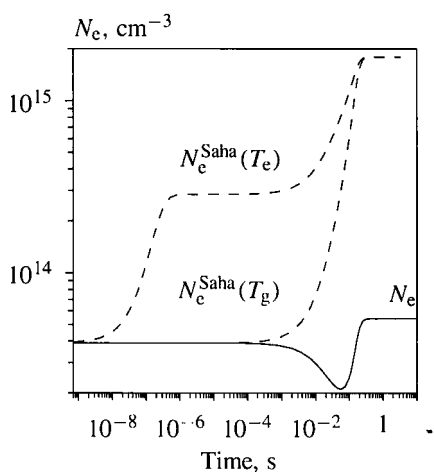
Depending on the value of intensity G , the laser radiation interaction with the evaporated material can proceed in two qualitatively different regimes. In the first one, the evaporated material turns into the state of a partially ionized gas with $\nu_{\text{en}} \gg \nu_{\text{ci}}$. In the second one, vapors pass into the state of complete or nearly complete ionization with $\nu_{\text{ei}} \gg \nu_{\text{en}}$.

The first regime is realized at an insufficiently high intensity of radiation. Main features of this regime in aluminum vapor at $G = 10^7 \text{ W/cm}^2$ are illustrated by the temporal dependences of excited-state densities of a neutral atom (Fig. 6a), the electron density (Fig. 6b), and the temperatures of electrons and ions (Fig. 6c). The same dependences for copper vapor radiated at the intensity $G = 10^8 \text{ W/cm}^2$ are given in Fig. 7a–c.

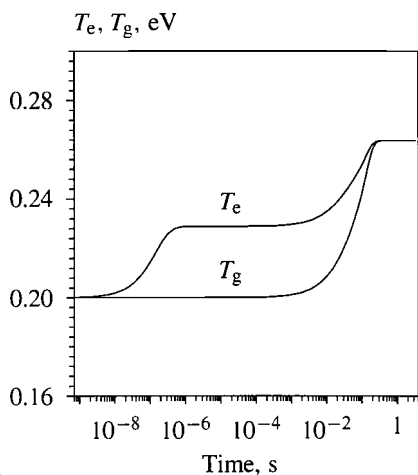
Let us consider the general pattern of the processes. At the onset, the evaporated substance is in the local-thermodynamic-equilibrium state and has the temperature T_0 and the density ρ_0 , and the corresponding concentrations of electrons N_e and excited states N_j . The electrons gain energy of the laser radiation field in electron–neutral collisions, but the process is slow because of low intensity G . At the beginning, till $t \approx 10^{-8} \text{ s}$ there are no visible changes in the densities and temperatures shown in Figs. 6 and 7. Then, during the time period determined by the values A_j^{-1} (Δt between about 10^{-8} and 10^{-7} s), the intensive radiation decay of the excited states occurs. For the Al vapor, densities of the lower most populated states decrease by 2–3 orders of magnitude, and for the Cu vapor by an order of 1 to 1.5. As the densities of excited states decrease, it becomes easier for electrons to gain energy. The temperature of electrons in the aluminum vapor rises from 0.2 to 0.24 eV. For the copper vapor the temperature increases from 0.2 to 0.276 eV because energy losses in elastic collisions are lower. For the temperatures reached, processes of



a

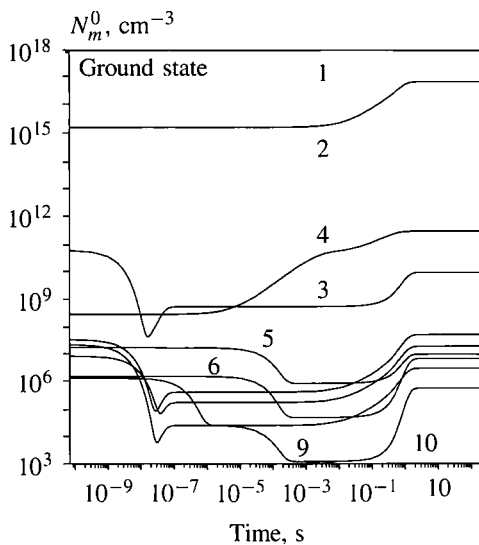


b

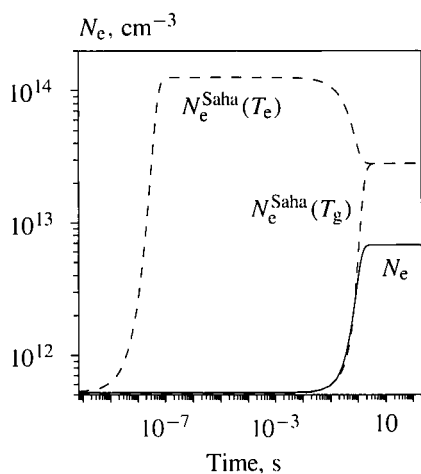


c

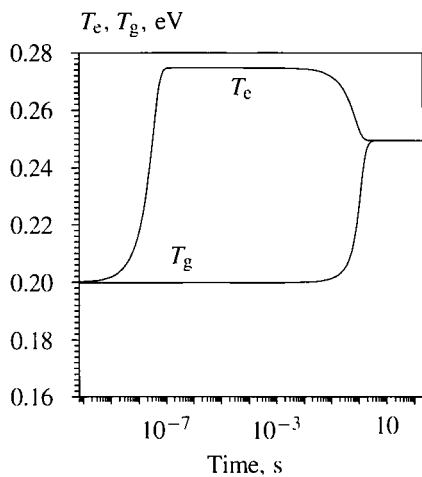
Fig. 6a-c. Aluminum vapor at $G = 10^7 \text{ W/cm}^2$. **a** Populations of ground and excited levels of neutral atom. Initial density of vapor $N_0^0 = 6 \cdot 10^{18} \text{ cm}^{-3}$ and initial temperature of vapor $T_0 = 0.2 \text{ eV}$. The curves are numbered according to the numbering of excited levels in Table 1. **b** Electron concentration in Al vapor predicted by the collision-radiation model (solid line) and electron concentrations calculated from the Saha equations for temperatures T_e and T_g (dashed lines). **c** Temperatures of electrons T_e and heavy particles T_g



a



b



c

Fig. 7 a–c. Copper vapor at $G = 10^8 \text{ W/cm}^2$. **a** Populations of ground and excited levels of neutral atom. Initial density of vapor $N_0^0 = 8 \cdot 10^{17} \text{ cm}^{-3}$ and initial temperature of vapor $T_0 = 0.2 \text{ eV}$. The curves are numbered according to the numbering of Table 2. **b** Electron concentration in Cu vapor predicted by the collision-radiation model (solid line) and electron concentrations calculated from the Saha equations for temperatures T_e and T_g (dashed lines). **c** Temperatures of electrons T_e and heavy particles T_g

spontaneous decay are equilibrated by collisional processes, see plateaus in Figs. 6 and 7 at Δt between about 10^{-6} and 10^{-3} s. Let us point out that during this period the contribution of ionization is minimal and N_e remains practically unchanged. By

the time moment $t \approx 10^{-1}$ s the triple-recombination process becomes dominant, which manifests itself in an N_e decrease and increases of N_j and T_e .

The energy balance of heavy particles (atoms and ions) remains practically the same and the thermodynamic equilibrium is violated in both substances since $T_e > T_g$. The increase of the temperature T_e results in a mutual compensation of excitation and deexcitation reactions. The balance of these reactions, however, is achieved when the values of the excited-state densities are one or two orders smaller than the initial ones (Figs. 6a and 7a).

In the aluminum vapor the recombination proceeds more intensively, which is demonstrated by a significant decrease of $N_e(t)$ (Fig. 6b) and a further growth of the temperature T_e (Fig. 6c) under the influence of the released energy. Increasing electron temperature not only restricts the recombination but causes excited states to be intensively populated and, hence, the avalanche ionization to be intensified (Fig. 6b). Owing to higher values of T_e and G , the influence of the recombination in the copper vapor is not equally noticeable and it plays mainly an equalizing role in the avalanche ionization processes. In the dependences given in Fig. 7b and c, this is revealed as the fast growth of N_e and the reduction of T_e .

At the second stage, the temperatures T_e and T_g gradually become equalized. Upon reaching the thermodynamic equilibrium, the system as a whole attains a stationary state at which all the processes appear to be mutually balanced, the laser action being compensated by a spontaneous radiative decay of excited states. In full-scale experiments this effect can be revealed as a rather powerful radiation flux, which is sometimes erroneously identified as a laser plasma. Mathematical modeling shows that, if spontaneous transitions are not taken into consideration, $A_{mj} = 0$, the system (5)–(11) has no stationary solutions at the intensity range considered. Comparison of the obtained equilibrium concentrations of electrons N_e (Figs. 6b and 7b) and excited particles N_m^0 (Figs. 6a and 7a) shows that they differ significantly from the values derived from the Saha–Boltzmann equations (14)–(16). Calculations show that these differences may be of one or two orders of magnitude, depending on the intensity and duration of laser radiation.

Thus, laser action regimes with intensities insufficient for optical breakdown are represented by a complicated pattern of nonequilibrium interconnected processes which are eventually responsible for the optical properties and radiative capability of a partially ionized vapor. Although, if the laser action is long enough, the system reaches the thermodynamic equilibrium, but its parameters do not coincide with the Saha–Boltzmann ones because of a powerful spontaneous radiation. Thereby the Saha–Boltzmann description turns out to be inadequate to describe the optical properties of the laser plume.

As the laser intensity G increases, so do the values of N_e , N_m^+ , T_e , T_g , and ν_{ei} . The relation between the frequencies ν_{en} and ν_{ei} remains the same ($\nu_{en} \gg \nu_{ei}$) approximately up to $G \sim 10^7$ W/cm² in the aluminum vapor (Fig. 8) and $G \sim 10^9$ W/cm² in the copper vapor (Fig. 9). At a sufficiently high intensity ($3 \cdot 10^7$ W/cm² for the Al vapor, $2 \cdot 10^9$ W/cm² for the Cu vapor) the density of charged particles becomes so

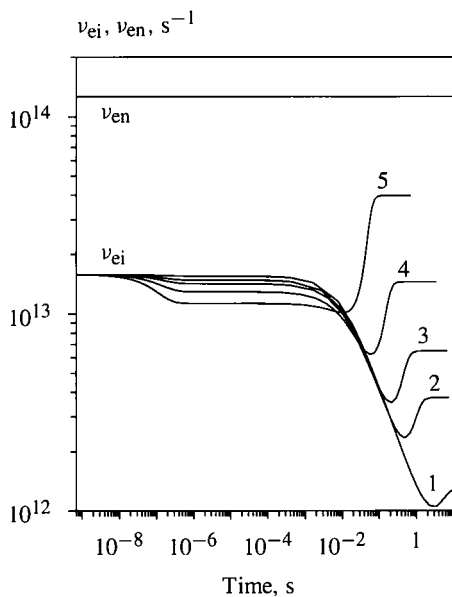
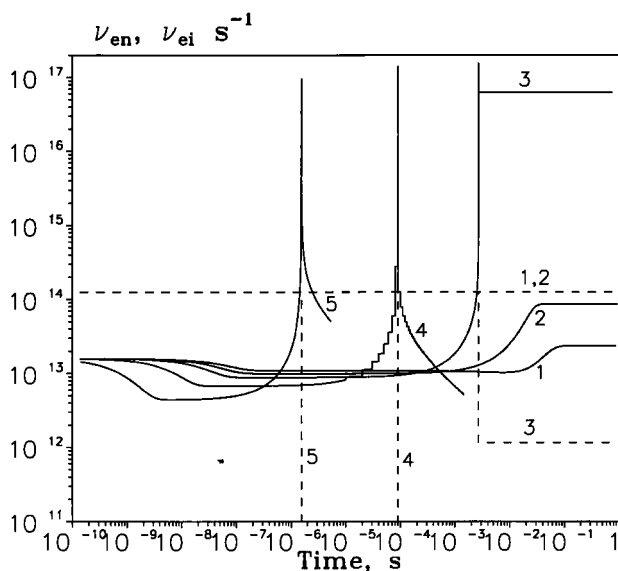
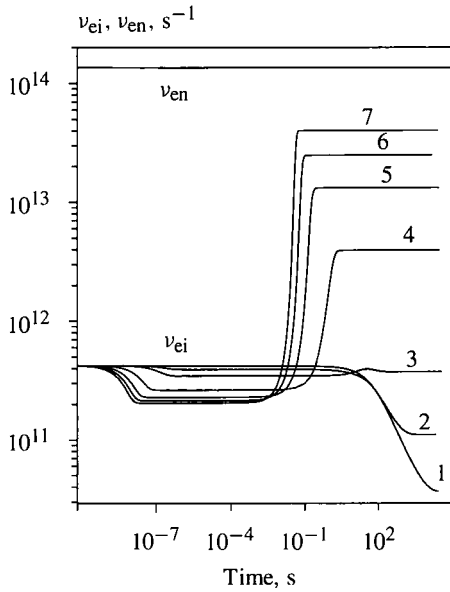
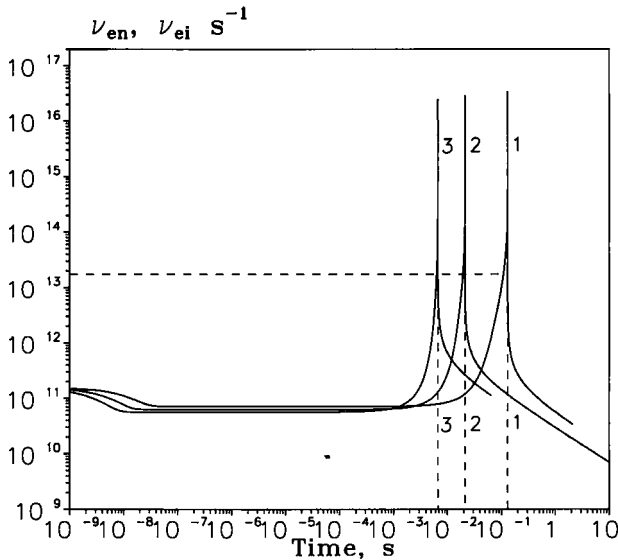
**a****b**

Fig. 8 a, b. Frequencies of electron–neutral ν_{en} and electron–ion ν_{ei} collisions in Al vapor calculated at initial density $N_0^0 = 6 \cdot 10^{18} \text{ cm}^{-3}$, initial temperature $T_0 = 0.2 \text{ eV}$ and the following values of laser radiation intensity G : **a** $1 \cdot 10^6 \text{ W/cm}^2$, $2.3 \cdot 10^6 \text{ W/cm}^2$, $3.5 \cdot 10^6 \text{ W/cm}^2$, $4 \cdot 10^7 \text{ W/cm}^2$, $5 \cdot 2 \cdot 10^7 \text{ W/cm}^2$; **b** $3 \cdot 10^7 \text{ W/cm}^2$, $2.5 \cdot 10^7 \text{ W/cm}^2$, $3 \cdot 10^8 \text{ W/cm}^2$, $4.5 \cdot 10^8 \text{ W/cm}^2$, $5 \cdot 10^9 \text{ W/cm}^2$



a



b

Fig. 9a, b. Frequencies of electron-neutral ν_{en} and electron-ion ν_{ei} collisions in Cu vapor calculated at initial density $N_0^0 = 8.3 \cdot 10^{17} \text{ cm}^{-3}$, initial temperature $T_0 = 0.2 \text{ eV}$ and the following values of laser radiation intensity G : **a** $1 \cdot 10^6 \text{ W/cm}^2$, $2.3 \cdot 10^6 \text{ W/cm}^2$, $3 \cdot 10^7 \text{ W/cm}^2$, $4 \cdot 10^8 \text{ W/cm}^2$, $5.3 \cdot 10^8 \text{ W/cm}^2$, $6.5 \cdot 10^8 \text{ W/cm}^2$, $7.7 \cdot 10^8 \text{ W/cm}^2$; **b** $2 \cdot 10^9 \text{ W/cm}^2$, $2.5 \cdot 10^9 \text{ W/cm}^2$, $3 \cdot 10^{10} \text{ W/cm}^2$

high that the frequency of Coulomb collisions becomes comparable with and then quickly exceeds that of electron–neutral collisions ($\nu_{ei} > \nu_{en}$) (Figs. 8b and 9b).

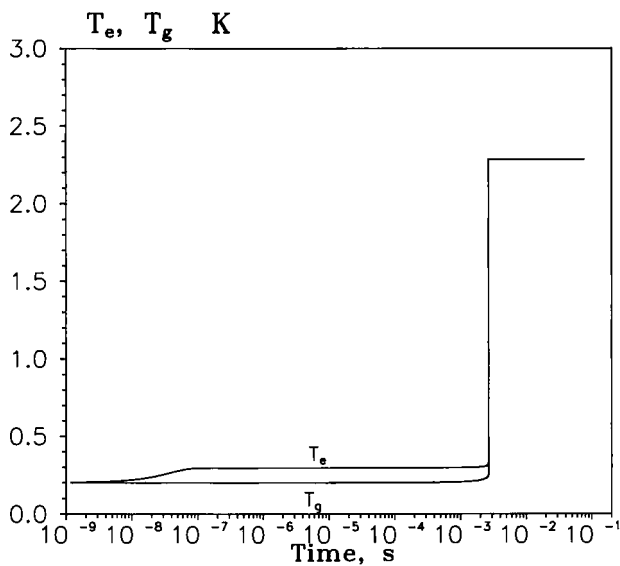
4.2 Optical breakdown

Temporal dependences of the temperatures T_e and T_g and the electron concentration N_e calculated at the intensities $G = 10^8 \text{ W/cm}^2$ for Al and $G = 5 \cdot 10^9 \text{ W/cm}^2$ for Cu are presented in Figs. 10–12.

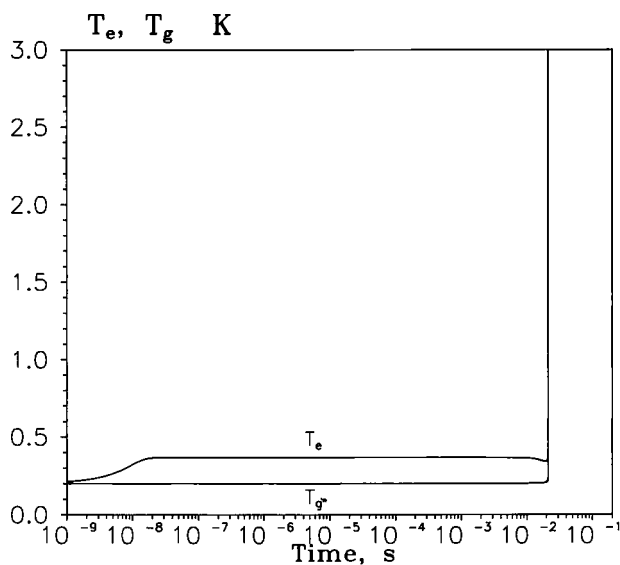
Let us define two threshold values of intensity as the lower and higher thresholds of breakdown. The lower breakdown threshold is the value of the radiation intensity at which collision frequencies become approximately equal, $\nu_{ei} \approx \nu_{en}$. The action duration in this case is not restricted beforehand. In other words, the lower breakdown threshold presents a minimum possible value of the intensity that, however, can induce the electron-ionic avalanche development. But the time necessary for the avalanche to develop can turn out to be unrealistically long as compared to the actual laser pulse duration. Therefore, the notion of a higher breakdown threshold is introduced as the minimum radiation intensity that will induce the avalanche at a specified and fixed pulse duration.

The avalanche development of optical breakdown is characterized by the domination of electron excitation and the step-by-step ionization of a neutral atom. With this taken into account, the dynamics of optical breakdown can conventionally be divided into two stages. At the beginning of the first stage, the electrons rapidly gain energy in the laser radiation field, colliding mainly with neutral atoms, $\nu_{ei} \ll \nu_{en}$. The energy exchange between the electron subsystem and heavy particles is slow because of the great difference between the mass of the electron m and that of the atom M , m/M being in the range of 10^{-4} to 10^{-5} . Therefore the electron temperature T_e at this stage is much higher than the vapor temperature T_g (Fig. 10). At this stage nearly all the electron energy is expended to fill the excited levels. Ionization losses are not great because of the low rate of ionization limited by the electron temperature $T_e \ll 1 \text{ eV}$. As long as the relation $\nu_{en} \gg \nu_{ei}$ is fulfilled, the electron temperature does not change because the acquisition of energy by electrons is compensated by excitation losses. As the density of excited states and charged particles increases, so does the frequency of Coulomb collisions. This is the slowest stage of the avalanche ionization process. Once the value ν_{ei} becomes compatible with the frequency of electron–neutral collisions, the electron temperature begins to grow rapidly. The avalanche ionization enters the fast stage at which the charged-particle concentrations increase by several orders of magnitude (Fig. 11) and as a result the energy exchange between the subsystems is accelerated.

Another peculiarity of the temperature evolution is the behavior of T_e after the avalanche ionization has been completed: if the intensity is not very high ($G < 3 \cdot 10^8 \text{ W/cm}^2$ for Al), the temperature becomes stationary. At such an intensity the maximum electron temperature can be as high as about 3 eV, which is sufficient for



a



b

Fig. 10. Temperatures of electrons T_e and heavy particles T_g calculated in Al vapor at the laser radiation intensity $G = 10^8 \text{ W/cm}^2$ (a) and $G = 5 \cdot 10^9 \text{ W/cm}^2$ (b)

the total ionization of neutral atoms and single- or twice-ionized particles. At higher intensities, due to a limited number of ions taken into account by the model, the temperature can rise indefinitely.

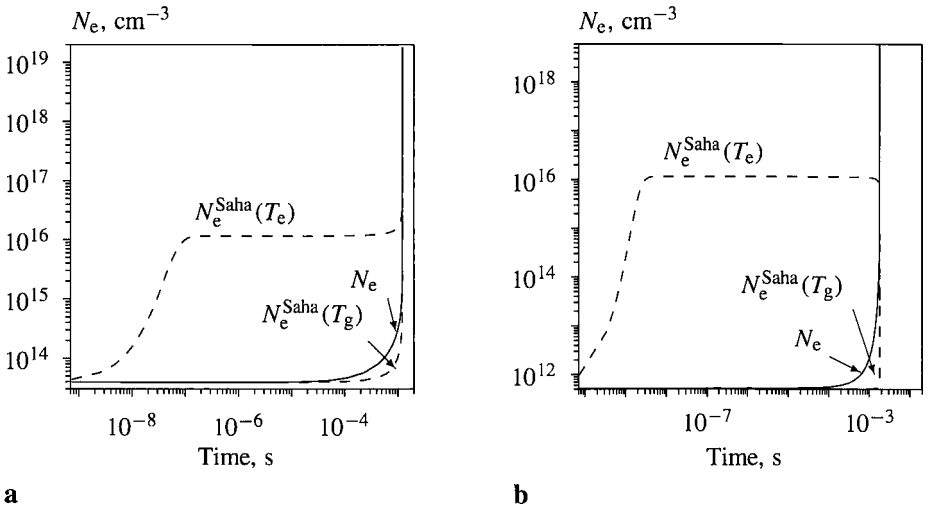


Fig. 11. Electron concentration in vapors predicted by the collision-radiation model (solid line) and electron concentrations calculated from the Saha equations for temperatures T_e and T_g (dashed lines). **a** Aluminum ($G = 10^8 \text{ W/cm}^2$), **b** copper ($G = 5 \cdot 10^9 \text{ W/cm}^2$)

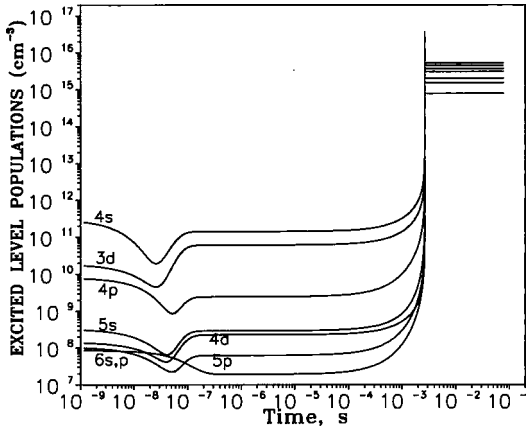


Fig. 12. Populations of electron levels $N_m^0(t)$ of the neutral Al atom under the action of laser radiation with the intensity $G = 10^8 \text{ W/cm}^2$

The evolutions of the electron concentration N_e in the Al vapor at the laser radiation intensity $G = 10^8 \text{ W/cm}^2$ and in the Cu vapor at $G = 5 \cdot 10^9 \text{ W/cm}^2$ are shown in Fig. 11. For both substances the temporal dependences of the concentrations of electrons and ions calculated by the kinetic model are compared with the values found for the two temperatures T_e and T_g from the Saha equations. The comparison shows that the curves determined by the kinetic model lie between two equilibrium curves $N_e^{\text{Saha}}(T_e)$ and $N_e^{\text{Saha}}(T_g)$ at $T_e \neq T_g$ and completely coincide when the temperatures become equal $T_e \simeq T_g$.

Thus, the comparison of the curves $N_e(t) = \sum_{z=1}^{z_{\max}} (N_0^z)$, $N_e^{\text{Saha}}(T_e)$, and $N_e^{\text{Saha}}(T_g)$ points to a strongly nonequilibrium avalanche ionization which is due to the difference between the temperatures of the two subsystems. In the optical-breakdown regime the radiation transitions are of little significance, since the frequency of Coulomb collisions ν_{ei} appears to be much higher than that of electron–neutral collisions $\nu_{ei} \gg \nu_{en}$ and that of the spontaneous decay of excited states $\nu_{ei} \gg A_{mj}^z$. Therefore, once the system reaches the thermodynamic equilibrium, the plasma charge composition coincides completely with the Saha–Boltzmann distribution.

The evolution of excited-level concentrations of a neutral atom in the Al vapor irradiated with an intensity exceeding the threshold one is shown in Fig. 12. At $t \simeq 10^{-8}$ s one can observe the intensive spontaneous radiative decay of the excited states of the atom, due to which the concentration of atoms in excited states diminishes and that of the atoms in the ground state grows. This can be observed in Fig. 12 in the form of a trough in the values of excited-state populations. Later on, as the electron temperature T_e rises, excitation and deexcitation by electron impacts start to play an important role. The populations start to increase gradually before the moment of optical breakdown and then rise sharply and approach steady-state values.

Calculations show that the threshold intensities of optical breakdown for the Al and Cu vapors differ by about two orders and are equal to $G_0 = 3 \cdot 10^7$ W/cm² for Al and $G_0 = 2 \cdot 10^9$ W/cm² for Cu. On the other hand, the optical-breakdown durations for Al and Cu for near-threshold radiation intensities and an unlimited laser pulse duration are comparable and equal to $t_0 = 3 \cdot 10^{-2}$ s and $t_0 = 10^{-2}$ s, respectively. These facts can be explained by special features of the electron shell configurations and by different ionization potentials of the neutral Al and Cu atoms, which will be considered below.

4.3 Influence of electron shell structure and ionization potential on threshold values of radiation intensity and duration

To estimate the influence of the electronic configuration and the ionization potential of a neutral atom on the principal characteristics of the optical breakdown let us perform a computational experiment, where the value of the neutral Al atom ionization potential $J_0^0 = 5.98$ eV will be raised up to that of the Cu atom $J_0^0 = 7.7$ eV. Conversely, the Cu atom ionization potential will be lowered down to the value of the Al atom one. The increase in the ionization potential $J_0^0(\text{Al})$ is accompanied by a growth of the intensity threshold values (Fig. 13 a), and at $J_0^0(\text{Al}) = 7.7$ eV the value of G_0 reaches $4 \cdot 10^8$ W/cm². This is approximately 5 times lower than the intensity required for the Cu vapor breakdown under the same conditions. Hence, at the same values of the ionization potentials $J_0^0(\text{Al}) = J_0^0(\text{Cu}) = 7.7$ eV the intensity threshold values remain essentially different. This is connected with the particular electron configurations of the atoms. This conclusion is confirmed by

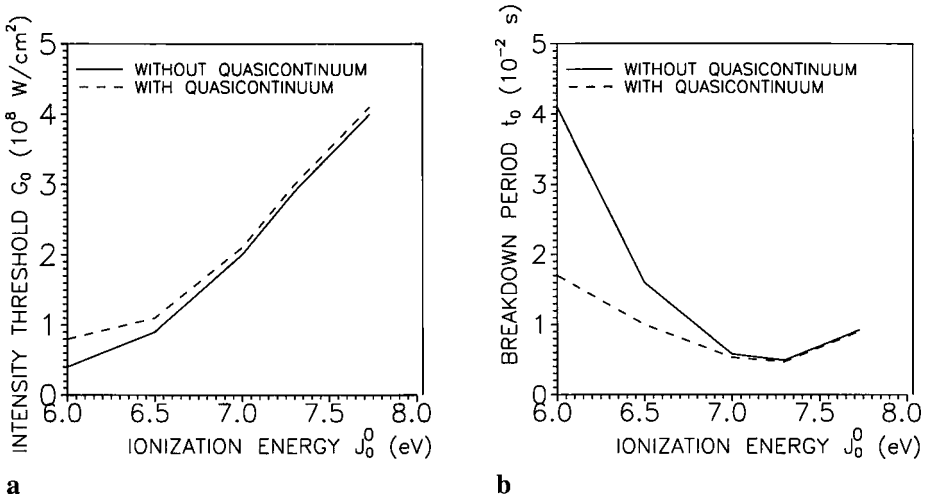


Fig. 13. Dependences $G_0(J_0^0)$ of the laser radiation intensity threshold values (a) and $t_0(J_0^0)$ of the breakdown time values (b) on the ionization potential of the Al neutral atom calculated without quasicontinuum being taken into account (solid line) and with quasicontinuum (dashed line)

simulation of breakdown in the Cu vapor when the ionization potential $J_0^0(\text{Cu})$ is lowered to $J_0^0(\text{Al})$. At $J_0^0(\text{Cu}) = 5.9$ eV the threshold values of G_0 are found to be 4 times higher than those for the Al vapor. The breakdown duration decreases as the ionization potential J_0 increases (Fig. 13b) because of the higher threshold values of the intensity.

Influence of the resonance level position

As noted above, the electron shells of the Al and Cu atoms have significant differences. First of all, in the Al atom, whose ionization potential is about 1.7 eV lower than that of the Cu atom, the resonance level is approximately twice as high as the first excited state in the Cu atom. Moreover, the resonance level in the Cu atom is metastable, i.e., the optical transition from this state to the ground state is forbidden.

In order to study the dependences of the main characteristics of the optical breakdown on the position of the resonance level in the Al atom, we shall use a simplified scheme of the electron structure of the atom. The vapor will be considered as an ideal two-level monatomic gas, in which particles can be only at one of the three states: the ground state with the concentration N_0^0 , the first excited state (N_1^0), and the single-charged state ($N_0^1 = N_e$). Furthermore, in the mathematical model under consideration we shall vary the resonance level excitation energy ΔE_{01}^0 from 0 to the values corresponding to the atom ionization potential J_0^0 and also vary the J_0^0 quantity itself. Then the threshold intensity values G_0 and the avalanche duration t_0 are determined from the simplified version of the system (5)–(11).

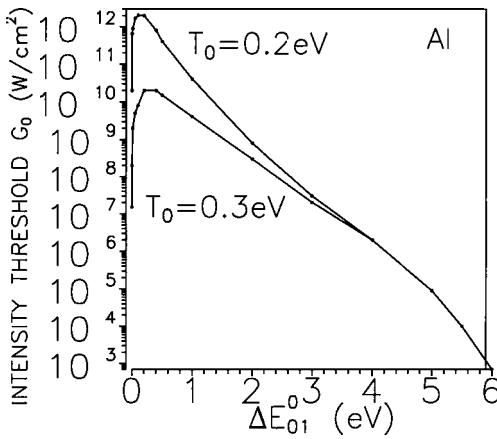


Fig. 14. Dependence $G_0(\Delta E_{01}^0)$ of the laser radiation intensity threshold values versus excitation energy of the Al neutral atom resonance level; $\Delta E_{01}^0(\text{Al}) = 3.14 \text{ eV}$

Figure 14 represents the dependence of the threshold intensity G_0 on the resonance level excitation energy of the neutral Al atom at two initial temperatures of the vapor. When the resonance level position is shifted from its real position $\Delta E_{01}^0(\text{Al}) = 3.14 \text{ eV}$ towards the ionized continuum $\Delta E_{01}^0 \rightarrow J_0^0$, the threshold intensity values are decreased by about three orders. The shift towards the ground state $\Delta E_{01}^0 \rightarrow 0$ results in a rapid growth of the threshold intensity values. Depending on the initial temperature the maximum increase is about three orders for $T_0 = 0.3 \text{ eV}$ and about five orders for $T_0 = 0.2 \text{ eV}$. The maximum values of G_0 are observed at the excitation energy $\Delta E_{01}^0 = 0.1 \text{ eV}$. When the ground and resonance levels are brought closer together, the threshold intensity decreases sharply. To explain the observed relation between the resonance level excitation energy and the threshold intensity of optical breakdown, let us analyze the electron energy variation due to the electron excitation and deexcitation as well as ionization and recombination reactions at laser radiation intensities in the vicinity of the threshold intensity G_0 .

Figure 15 gives the values of $Q_{0,1}^{\Delta E}$ (12) electron energy variation due to electron excitation and deexcitation reactions of resonance level for the Al vapor in the case when the laser radiation intensity $G = G_0 - \delta G$, where δG is small as compared to G_0 ($\delta G/G_0 \sim 0.01$). As noted above, in this case after a certain time the system comes to equilibrium with the external laser radiation and all the processes become steady. Since the electron-ion avalanche does not develop under such conditions, energy losses of electrons due to ionization of atoms are negligible. Most losses of the electron energy are connected with the electron excitation of the atom resonance state.

As has been noted, the principal difference of the electron shell structure of the Cu atom from that of the Al atom is that the resonance state in copper is metastable and the probability of radiative decay of this state into the ground state is small. Besides,

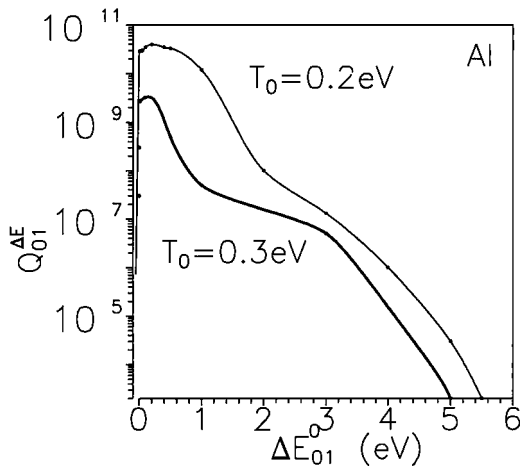


Fig. 15. Dependence $Q_{0,1}^{\Delta E}(\Delta E_{01}^0)$ characterized the electron component energy losses due to reactions of excitation and deexcitation of the resonance level of the Al neutral atom

the probability of the formation of an atom in the resonance state by collision of a Cu atom in the ground state with an electron is much smaller than that of the formation of an atom in the second excited state. Also the transition of the Cu atom into the metastable resonance state is favored not only by collision transitions but also by spontaneous radiative decay of the second excited state. Thus, in the Cu vapor the values of the threshold radiation intensity G_0 and the breakdown time t_0 are both dependent on the energy of the resonance level ΔE_{01}^0 and the second level ΔE_{02}^0 .

In order to determine what level has a greater effect on the G_0 and t_0 values, two series of calculations are performed on the model with only two excited levels being taken into account: in the first series the excitation energy of the second level ΔE_{02}^0 is fixed and the excitation energy of the metastable resonance state ΔE_{01}^0 is varied; in the second series the energy ΔE_{01}^0 is fixed and the energy ΔE_{02}^0 is varied. The calculation results are given in Fig. 16. It can be seen that the excitation energy of the metastable state exerts a weak influence on the threshold intensity G_0 , whereas the energy of the second excited state (with the optical transition from this state to the ground one being permitted) exerts a stronger effect on the value of G_0 . In addition, the behavior of the dependence $G_0(\Delta E_{02}^0)$ coincides qualitatively with a similar dependence $G_0(\Delta E_{01}^0)$ for the Al vapor (Fig. 14).

The results obtained indicate that in order to initiate the optical breakdown in the vapor of a metal whose atoms have electron levels with small excitation energies, it is necessary to use a laser radiation with a higher intensity than that used to initiate the breakdown of atoms with excited state being positioned at higher energies. The presence of metastable levels also makes a contribution to the optical-breakdown dynamics.

Now we shall analyze the variation in the breakdown duration $t_0(\Delta E^0)$ versus

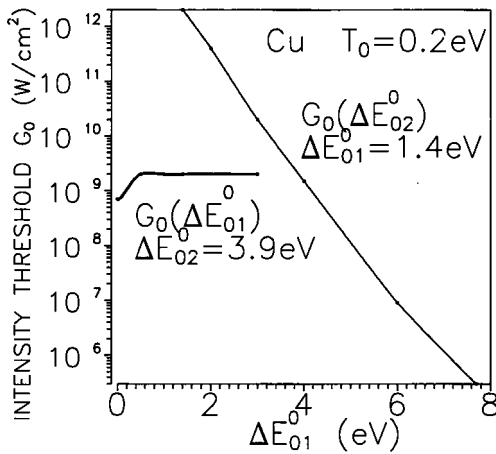
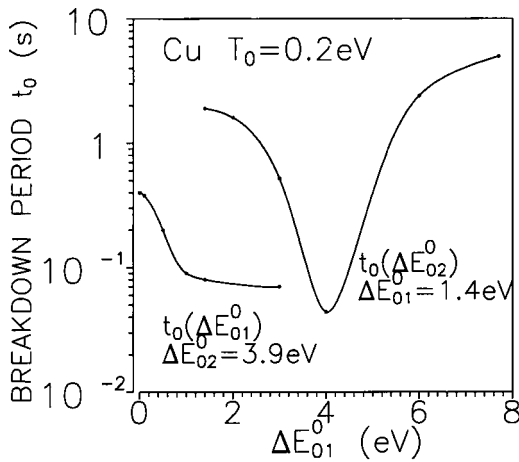


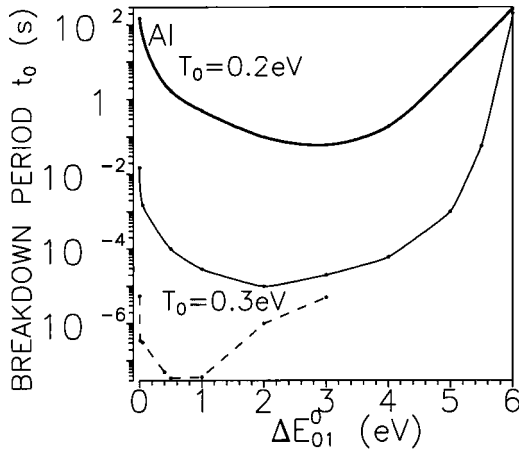
Fig. 16. Dependence $G_0(\Delta E_{0m}^0)$, $m = 1, 2$, of the laser radiation intensity threshold values on the excitation energies of the 1st and 2nd excitation levels of the Cu neutral atom

the excitation energy of the resonance electron state of the neutral atoms of Al and Cu. These dependences calculated at the threshold laser radiation intensity $G = G_0(\Delta E^0)$ are presented in Fig. 17a for the Cu vapor and in Fig. 17b for the Al vapor. To understand the reasons for the difference in the breakdown durations for different excitation energies of the resonance state of a neutral atom, it is necessary to analyze the dynamics of the development of the electron-ion avalanche from the beginning of the laser action on the metal vapor.

As shown above (Fig. 15), at small resonance state excitation energies ΔE_{01}^0 at the stage preceding the emergence the electron-ion avalanche, the major fraction of the electron energy is spent to excite the resonance state. As a consequence, the resonance level is rapidly populated. The ionization rate of this level is low because of the high ionization energy $J_1^0 = J_0^0 - \Delta E_{01}^0$. Due to the latter circumstance the electron-ion avalanche develops slowly. With increasing ΔE_{01}^0 the resonance level is populated not so intensively as in the case of small ΔE_{01}^0 , electron energy losses due to excitation diminish, but the ionization rate grows. In this connection the time taken for the avalanche to develop is decreased and reaches the minimum value at $\Delta E^0 \sim J_0^0/2$ (Fig. 17). As ΔE^0 grows above $J_0^0/2$, the small resonance state excitation rate begins to decelerate significantly the population process, which leads to decelerating the electron-ion avalanche development regardless of the fact that the ionization rate of this state grows rapidly. As a result of the mutual action of these two processes the breakdown durations for the Al and Cu vapors are increasing as the excited state approaches the ionization continuum. When the initial temperature of the vapor increases up to $T_0 = 0.3$ eV, the dependence $t_0(\Delta E^0)$ does not vary qualitatively. The excitation energy of the metastable electron level of the Cu atom has only a weak influence on the duration of optical breakdown (Fig. 17a).



a



b

Fig. 17. Dependence of the breakdown time on the excitation energies of the resonance states of Cu (a) and Al (b) neutral atoms. a $t_0(\Delta E_{0m}^0)$, $m = 1, 2$, for the 1st and 2nd excitation levels of the Cu neutral atom. b $t_0(\Delta E_{01}^0)$ for different initial temperatures (solid lines) and with allowance for higher-excited states (dashed line)

Influence of higher-excited states

The behavior of $G_0(\Delta E^0)$ and $t_0(\Delta E^0)$ is changed if other excited states of neutral atom, beside the resonance one, are also taken into account. Calculations for the Al vapor on the basis of the model with 10 excited states of the neutral atom taken into account show that in this case the step-by-step ionization of excited states exerts a considerable influence on the formation of the electron-ion avalanche, decreasing the duration of ionization by several orders (Fig. 17b, the resonance level excitation

energy ΔE_{01}^0 varies from 0 to $\Delta E_{02}^0(\text{Al})$). In addition, the minimum of the breakdown period $t_0(\Delta E_{01}^0)$ is shifted from the $\Delta E_{01}^0 \sim J_0/2$ point towards lower values and occurs at $\Delta E_{01}^0 \sim 1$ eV. Also it should be pointed out that when higher-excited states are included into the model, this leads to an increase of the threshold values of the laser radiation intensity G_0 .

The result obtained indicates that higher-excited states have a significant effect on the duration of optical breakdown and the threshold radiation intensity and should be taken into account when developing the collision-radiation model.

Highly excited states $m > M^z$ can be included into the model by means of the quasicontinuum approximation. The influence of the quasicontinuum is noticeable for the calculations of the threshold values of optical breakdown and the steady-state values of charged-particle densities in the laser plasma. So far the influence of the quasicontinuum on the optical-breakdown dynamics has not been clarified. It is commonly assumed that the role of the quasicontinuum is negligible because the ion distribution in the course of optical breakdown is much lower than the equilibrium one.

The influence of the quasicontinuum on the characteristics of the optical breakdown is similar to that of the introduction of additional excited states into the collision-radiation model. Figure 13 a and b represents the $G_0(J_0^0)$ and $t_0(J_0^0)$ dependences of the threshold radiation intensity and the optical-breakdown duration on the ionization potential of the neutral atom. Calculations were performed for the Al vapor by the model with 10 excited levels with and without taking the quasicontinuum into account. The introduction of the quasicontinuum raises the intensity threshold values G_0 by about 2 times and decreases the avalanche duration t_0 by 2.5 times. As the ionization potential increases up to 7.7 eV, the influence of the quasicontinuum is diminished (Fig. 13). This is connected with the fact that the calculations are carried out with a constant number of excited states and, when the value of $J_0^0(\text{Al})$ is increased, a noticeable energy gap is formed between the last excited level and the ionization continuum. The results obtained indicate that in the optical-breakdown simulation the number of levels to be taken into account must be larger than (or equal to) 10. The influence of higher levels can be taken into account by the quasicontinuum model.

Also the quasicontinuum approximation significantly influences the laser plasma parameters when the system approaches its steady state. The calculations performed show that the quasicontinuum has only a weak influence on the results while the plasma is in the overheated and ionizationally nonequilibrium state and the populations of the excited levels are much smaller than the ones defined from the Boltzmann distribution. But the role of the quasicontinuum increases as the system approaches its equilibrium state. In this case the calculated values of concentrations are much different (by factors of 2–4) from the equilibrium distribution if the quasicontinuum is not taken into account.

4.4 Influence of initial temperature and irradiation duration

Let us consider the influence of two quantities, namely, the initial temperature $T_e(t)|_{t=0} = T_g(t)|_{t=0} = T_0$ and the laser action duration τ on the parameters of the optical breakdown (Fig. 18).

As the initial temperature T_0 grows, the vapor ionization enhances the initial concentrations of charged particles and, hence, the frequency ν_{ei} increases. In this way the relation $\nu_{ei} \gg \nu_{en}$ is achieved at considerably lower values of the threshold intensity G . As the initial vapor temperature T_0 rises from 0.2 eV to 0.4 eV, the value of the lower breakdown threshold becomes 2–10 times smaller.

At temperature $T_0 \geq 0.4$ eV the initial frequency of Coulomb collisions is found to be higher than the frequency of electron–neutral collisions $\nu_{ei} > \nu_{en}$, i.e., from the very beginning the evaporated substance is already in the plasma state. To establish a new equilibrium state in such situations, much shorter times and smaller intensities are required. Depending on the intensity applied, the breakdown duration at $T_0 = 0.4$ eV is shifted from the millisecond range to the micro- or nanosecond range.

Thus, the upper threshold values can be determined by the curves of Fig. 18. It should be noted that while the initial temperature T_0 increases, the predicted values of threshold intensities become closer to the experimental data [2, 11]. This demonstrates that, on the one hand, the kinetic models considered are applicable for the micro-level process description and, on the other hand, determine the direction of further analysis for physical processes that should be taken into account in more complex and completed models. Among the factors that can induce significant elevation of the evaporated-matter temperature are the energy release rate and conditions of gas-dynamic expansion under the presence of the external atmosphere.

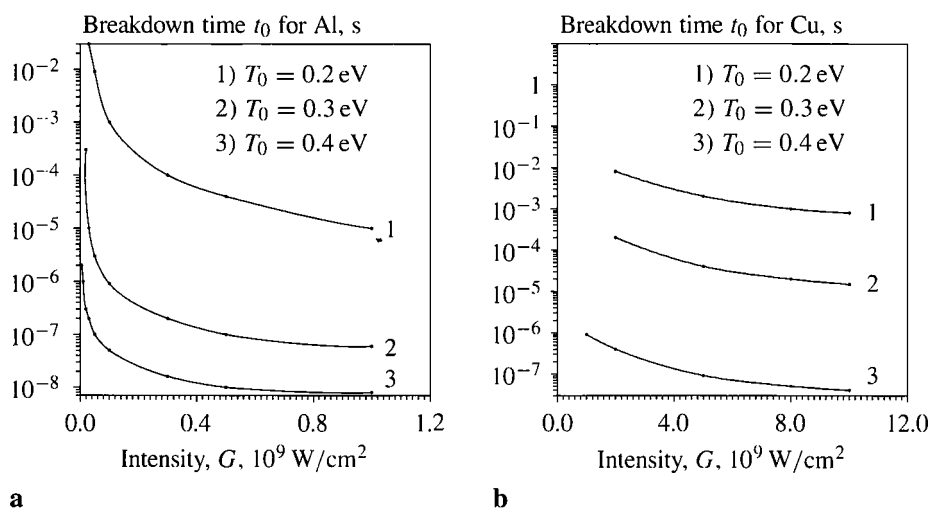


Fig. 18. Dependence $t_0(G_0)$ of breakdown time for Al (**a**) and Cu (**b**) on laser radiation intensity for the different values of the initial temperature of vapor T_0

5 Conclusion

The interaction of laser radiation and evaporated substance involves a number of highly nonequilibrium processes. The nonequilibrium of the processes is determined by fast absorption of the radiation energy in the electronic subsystem and the slow energy exchange between the subsystems. Depending on the duration and intensity of the radiation, the micro-level processes can proceed in two qualitatively different regimes: the prebreakdown regime and the optical-breakdown regime.

The prebreakdown regime is characterized by the violation of the equilibrium between the matter and the radiation. This leads to a deviation of the charge composition of the partially ionized gas from the Saha–Boltzmann distribution and indicates that it is unjustified to use equilibrium approaches for the determination of the optical vapor properties playing an important role in laser welding and some other applications. As a result of the optical breakdown, the evaporated substance passes to the near-equilibrium plasma state. The radiative transitions lose their importance because of the total domination of the collisional reactions. The charge composition can be determined from the equilibrium Saha equations.

The studies performed allow us to determine that it is the electronic shell structure of the matter that plays a determining role in the avalanche development, while the influence of ionization potentials is less significant. A comparative analysis of the optical breakdown in the Al and Cu vapors shows that atoms with lowly positioned excited states (Cu) have higher threshold values of radiation intensity. For example, G_{thres} for the Cu vapor is approximately by one order of magnitude higher than that for the Al vapor. In atoms with highly positioned levels of electronic excitation the optical breakdown proceeds at a lower radiation intensity, but the avalanche development duration is several times longer.

A detailed analysis of the optical-breakdown kinetics in aluminum and copper vapors shows that kinetic models for metal atoms should include not less than 10 excited states. The influence of higher excited states can be effectively accounted for by the quasicontinuum approximation. This statement is quite general and is exceedingly important for the correct description of the level population and the ionization kinetics in nonequilibrium radiative-gas dynamics problems.

The modeling performed for main features of the optical breakdown in aluminum and copper vapors confirms the threshold nature of this phenomenon and reveals its dependence on the intensity and the duration of the laser pulse and the medium temperature. Computations with varying initial temperatures show a good qualitative agreement with experimental data. However, quantitative coincidence should be expected if the target and the gas-dynamic phenomenon models will be taken into account.

Acknowledgement

Support of this work by RFBR, grant nr. 97-01-00942, is gratefully acknowledged.

References

1. Humphries, M., Kahbert, H. J., Pippert, K.: The excimer laser on its way to industrial application. In: Laude, L. D., Bauerle, D. (eds.): *Laser in manufacture*. Springer, London, pp. 200–210 (1987).
2. Danilov, E. D., Danilychev, V. A., Dolgykh, V. D., Evstigneev, V. V., Yakovlenko S. I.: Is-parenije mishenej i obrazovanije voln pogloschenija v vozdukh pri vozdeystvii ultrafioletovogo lazernogo izluchenija. *Kvantovaja Electron. (Moscow)* 15: 2568–2577 (1988).
3. Weyl, G. M., Rosen, D. I.: Laser-induced breakdown in argon at 0.35 μm : theory and experiment. *Phys. Rev. A* 31: 2300–2313 (1985).
4. Kadawa, K., Yokoi, S., Nakajima, S.: Metal plasma induced by the bombardment of 308 nm excimer and 585 dye laser pulses at low pressure. *Opt. Commun.* 45: 261–265 (1983).
5. Chenais-Popovics, C., Renaudin, P., Rancu, O., Gilleron, F., Gauthier, J.-C., Larroche, O., Peyrusse, O., Dirksmoller, M., Sondhauss, P., Missalla, T., Uschmann, I., Forster, E., Renner, O., Krousky, E.: Kinetic to thermal energy transfer and interpretation in the collision of laser-produced plasmas. *Phys. Plasmas* 4: 190–208 (1997).
6. Niedrig, R., Bostonjoglo, O.: Imaging and modeling of pulse laser-induced evaporation of metal films. *J. Appl. Phys.* 81: 480–485 (1997)
7. Gizzi, L. A., Giulietti, D., Giulietti, A., Afshar-Rad, T., Biancalana, V., Chessa, P., Danson, C., Schifano, E., Viana, S. M., Willi, O.: Characterisation of laser plasmas for interaction studies. *Phys. Rev. E* 49: 5628–5643 (1994).
8. Weyl, G., Pirri, A., Root, R.: Laser ignition of plasma off aluminum surfaces. *AIAA J.* 10: 460–469 (1981).
9. Mazhukin, V. I., Gusev, I. V., Smurov, I., Flamant, G.: Laser induced break-down of metals vapor. *Microchem. J. Special Issue "Laser in Analytical Chemistry"* 50: 413–433 (1994).
10. Rosen, D. I., Hastings, D. E., Weyl, G. M.: Coupling of pulsed 0.35 μm laser radiation to titanium alloys. *J. Appl. Phys.* 53: 5882–5890 (1982).
11. Rosen, D. I., Mitteldorf, J., Kothandarama, G., Pirri, A. N., Pugh, E. R.: Coupling of pulsed 0.35 μm laser radiation to aluminum alloys. *J. Appl. Phys.* 53: 3190–3200 (1982).
12. Ready, J. F.: *Effects of high-power laser radiation*. Academic Press, New York (1971).
13. Anisimov, S. I., Imas, Ya. A., Romanov, S. G., Khodyko, Yu. V.: *Action of high-power radiation on metals*. National Technical Information Service, Springfield, Va. (1971).
14. Arecchi, F. T., Sculz-Dubois, E. O.: *Laser handbook*, vol. 2. North-Holland, Amsterdam (1972).
15. Raizer, Yu. P.: *Laser induced discharge phenomena*. Consultant Bureau, New York (1977).
16. Mao, X., Chan, W.-T., Cactano, M., Shannon, M. A., Russo, R. E.: Preferential vaporization and plasma shielding during nano-second laser ablation. *Appl. Surf. Sci.* 96–98: 125 (1996).
17. Giuliani, J. L., Mulbardon, M., Hyman, E.: Structuring processes in expanding laser-produced plasmas. *Phys. Fluids B* 1: 1463 (1989).
18. Mazhukin, V. I., Smurov, I., Flamant, G.: Simulation of laser plasma dynamics: influence of ambient pressure and intensity of laser radiation. *J. Comput. Phys.* 112: 78–90 (1994).
19. McWriter, R. W. P., Hearn, A. G.: A calculation of the instantaneous population densities of the excited levels of hydrogen-like ions in a plasma. *Proc. Phys. Soc. Lond.* 82: 641–654 (1963).
20. Richter, J.: Radiation of hot gases (thermal and nonthermal). In: Lochte-Holtgreven, W.: *Plasma diagnostics*. North-Holland, Amsterdam, pp. 9–55 (1968).
21. Zeldovich, Ya. B., Raizer, Yu. P.: *Physics of shock waves and high temperature hydrodynamics phenomena*. Academic Press, New York (1967).
22. Holstein, T.: Imprisonment of resonance radiation in gases. *Phys. Rev.* 72: 1212–1225 (1947).
23. Biberman, L. M., Vorobjev, V. S., Yakubov, I. T.: *Kinetica neravnesnoj nizkotemperaturnoj plazmi*. Nauka, Moscow (1982).
24. Derzhiev, V. I., Zhydkov, A. G., Yakovlenko, S. I.: *Izluchenije ionov v neravnesnoj plotnoj plazme*. Energoatomizdat, Moscow (1986).

25. Von Allmen, M.: *Laser-beam interactions with materials: physical principles and application*. Springer, Berlin Heidelberg New York Tokyo (1981).
26. Krehl, P., Schwirzke, F., Cooper, A. W.: Correlation of stress-wave profiles and the dynamics of the plasma produced by laser irradiation of plane solid target. *J. Appl. Phys.* 46: 4400–4406 (1975).
27. Lokhudin, V. D., Samokhin, A. A.: O roli plazmi v processe intensivnogo isparenija metallov pri moshcnom lazernom vozdejstvii. *Fiz. Visok. Temp.* 15: 1152–1157 (1977).
28. Mazhukin, V. I., Pestrajakova, G. A.: Matematicheskoje modelirovanije poverkhnostnogo lazernogo isparenija. *Dokl. Akad. Nauk SSSR* 278: 843–847 (1984).
29. Mazhukin, V. I., Samarskii, V. V.: Mathematical modeling in the technology of laser treatments of materials. *Surv. Math. Ind.* 4: 85–149 (1994).
30. Ho, J. R., Grigoropoulos, G. P., Hemphrey, J. A. C.: Gas dynamics and radiation heat transfer in the vapor plume produced by pulsed laser irradiation of aluminum. *J. Appl. Phys.* 79: 7205–7215 (1996).
31. Le, H. C., Vuillon, J., Zeitoun, D., Marine, W., Sentis, M., Dreyfus, R. W.: 2D modeling of laser-induced plume expansion near the plasma ignition threshold. *Appl. Surf. Sci.* 96–98: 76–81 (1996).
32. Mazhukin, V. I., Smurov, I., Flamant, G., Surry, C.: Overheated metastable state in polymer sublimation by laser. *Appl. Surf. Sci.* 86: 7–12 (1996).
33. Schittenhelm, H., Callies, G., Berger, P., Hugel, H.: Investigations of extinction coefficients during excimer laser ablation and their interpretation in terms of Rayleigh scattering. *J. Phys. D* 29: 1564–1571 (1996).
34. Rykalin, N. N., Uglov, A. A., Zuev, I. V., Kokora, A. N.: *Lazernaja i electronno-luchevaja obrabotka*. Mashinostroyenie, Moscow (1980).
35. Pirri, A. N., Root, R. G., Wu, P. K. S.: Plasma energy transfer to metal surfaces irradiated by pulsed lasers. *AIAA J.* 16: 1296–1304 (1978).
36. Belouet, C.: Thin film growth by the pulsed laser assisted deposition technique. *Appl. Surf. Sci.* 96–98: 630–642 (1996).
37. Alunovic, M., Stamm, H., Aden, M., Kreutz, E. W.: Optical and particle properties of PLD vapour plasmas of ceramics. *Appl. Surf. Sci.* 96–98: 222–226 (1996).
38. Hermann, J., Boulmer-Leborgne, C., Dubreuil, B., Mihailescu, I. N.: Influence of irradiation conditions on plasma evaluation in laser-surface interaction. *J. Appl. Phys.* 74: 3071–3079 (1993).
39. Mazhukin, V. I., Gusev, I. V., Smurov, I., Flamant, G.: Line spectrum radiation transfer in nonequilibrium laser plasma of aluminum. In: McCay, T., Matsunawa, A., Huegel, H. (eds.): *Laser materials processing: ICALEO 94*. SPIE – the International Society for Optical Engineering, Bellingham, Wash., pp. 212–221 (1995).
40. Knight, C. J.: Theoretical modelling of rapid surface vaporization with back pressure. *AIAA J.* 17: 519–523 (1977).
41. Gudzenko, L. I., Yakovlenko, S. I.: *Plasmennije lazeri*. Atomizdat, Moscow (1978).
42. Stupitsky, E. L., Lubchenko, O. S., Rhdaverdyan, A. M.: Neravnovesnije processi pri razlete visokotemperaturnogo plazmennogo sgustka. *Kvantovaja Electron. (Moscow)* 12: 1038–1056 (1985).
43. Moore, C. E.: *Atomic energy levels, vol. 1*. National Bureau of Standards, Washington, D.C. (1971).
44. Venugopalan, M. (ed.): *Reactions under plasma conditions, vol. 1*. Wiley-Interscience, New York (1971).
45. Latter, R.: Temperature behavior of the Tomas-Fermi statistical model for atoms. *Phys. Rev.* 99: 378–385 (1955).
46. Rudge, M. R. H.: Theory of the ionization of atoms by electron impact. *Rev. Mod. Phys.* 40: 564–581 (1968).
47. Presnyakov, L. P., Urnov, A. M.: Asymptotic approach to the theory of excitation of multiply-charged ions by electron impact. *J. Appl. Phys. Atom. Mol. Phys.* 138: 1280–1287 (1975).

48. Vainshtein, L. A., Sobelman, I. I., Yukov, E. A.: Vozbuzhdenije atomov i ushirenije spectralnikh linij. Nauka, Moscow (1979).
49. Bazylev, V. A., Chibisov, M. I.: Electronnoje vozbuzhdenije i ionizacija mnogozaradnikh ionov. Usp. Fiz. Nauk 133: 617–643 (1981).
50. McWhirter, R. W. P., Hearn, A. G.: A calculation of the instantaneous population densities of the excited levels of hydrogen-like ions in a plasma. Proc. Phys. Soc. 82: 641–654 (1963).
51. Seaton, M. J. L.: The spectrum of the solar corona. Planet. Space Sci. 12: 55–63 (1964).
52. Lotz, W.: Electron-impact ionization cross-section for atoms up to $z = 108$. Zh. Fiz. 232: 101–112 (1970).
53. Van Regemorter, H.: Rate of collisional excitation in stellar atmospheres. Astrophys. J. 132: 906–913 (1962).
54. Allen, C. W.: Astrophysical quantities, 3rd edn. Athlone Press, London (1973).
55. Zaidel, A. I., Prokof'ev, V. K., Raisky, S. M.: Tablici spectralnikh linij. Nauka, Moscow (1977).
56. Wiese, W. J., Smith, M. W., Miles, B. M.: Transition probabilities, vol. 2. National Bureau of Standards, D.C. (1969).
57. Vainshtein, L. A., Sobelman, I. I., Yukov, E. A.: Electronnoje vozbuzhdenije atomov i ionov. Nauka, Moscow (1973).
58. Yakovlenko, S. I.: Radiacionnije i stolknovitelnije javlenija. Energoizdat, Moscow (1984).
59. Pitaevskij, L. P.: Electrons recombination in monatomic gas. Sov. Phys. JETP 42: 1326–1337 (1962).
60. Gear, C. W.: The numerical integration of ordinary differential equations. J. Math. Comput. 21: 146–156 (1967).
61. Byrne, C. D., Hindmarsh, A. C.: Stiff ODE solvers: a review of current and coming attractions. J. Comput. Phys. 70: 1–62 (1987).
62. Hairer, E., Norsett, S. P., Wanner, G.: Solving ordinary differential equation 1: nonstiff problems. Springer, Berlin Heidelberg New York Tokyo (1989).
63. Hairer, E., Wanner, G.: Solving ordinary differential equation 2: stiff problems. Springer, Berlin Heidelberg New York Tokyo (1991).
64. Gear, C. W.: DIFSUB for solution of ordinary differential equations. Commun. ACM 14: 185–190 (1971).
65. Hindmarsh, A. C., Byrne, C. D.: Applications of EPISOD: an experimental package for the integration of systems of ordinary differential equations. In: Lapidus, L., Schiesser, W. E. (eds.): Numerical methods for differential systems. Academic Press, New York, pp. 117–126 (1976).
66. Hindmarsh, A. C.: LSODE and LSODI: two new initial value ODE solvers. ACM SIGNUM Newsl. 15: 10–11 (1980).
67. Petzold, L. R.: Automatic selection of methods for solving stiff and nonstiff systems of ODE's. SIAM J. Sci. Stat. Comput. 1: 136–148 (1983).
68. Shirkov, P. D.: Metod rascheta khimicheskogo i ionizacionnogo ravnovesija v gazo-plazmennoj smesi. Mat. Model. 6: 97–123 (1991).

Authors' addresses: V. I. Mazhukin and V. V. Nossov, Institute of Mathematical Modeling, Russian Academy of Science, Miusskaya Ploschad 4, 125047 Moscow, Russia. – I. Smurov, Ecole Nationale d'Ingénieurs de Saint-Etienne, Saint-Etienne, France. – G. Flamant, Institut de Science et de Génie des Matériaux et Procédés, Centre National de la Recherche Scientifique, Font-Romeu, France.

Communicated by A. Samarskii